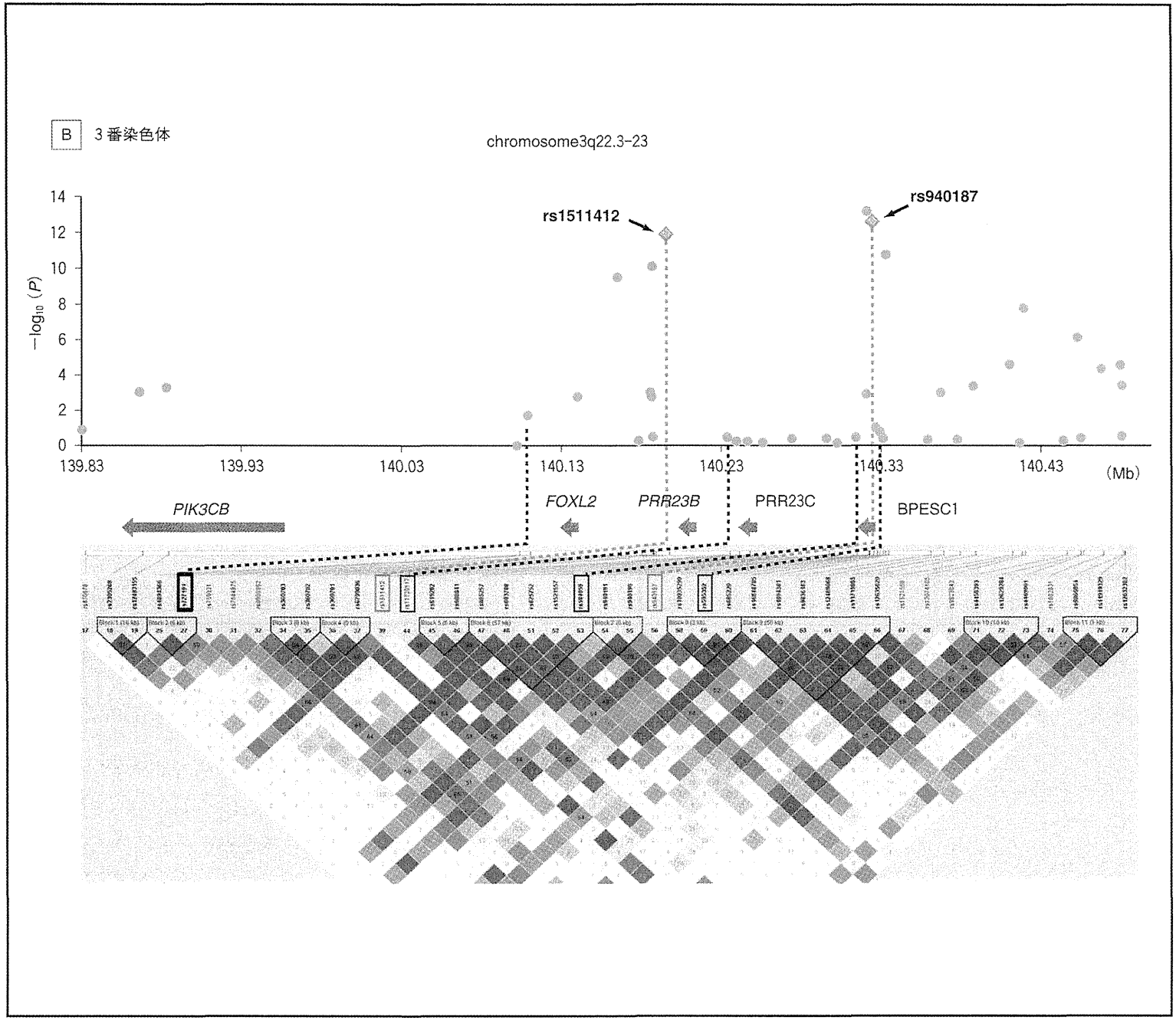

写真3　ケロイドに関連する3領域

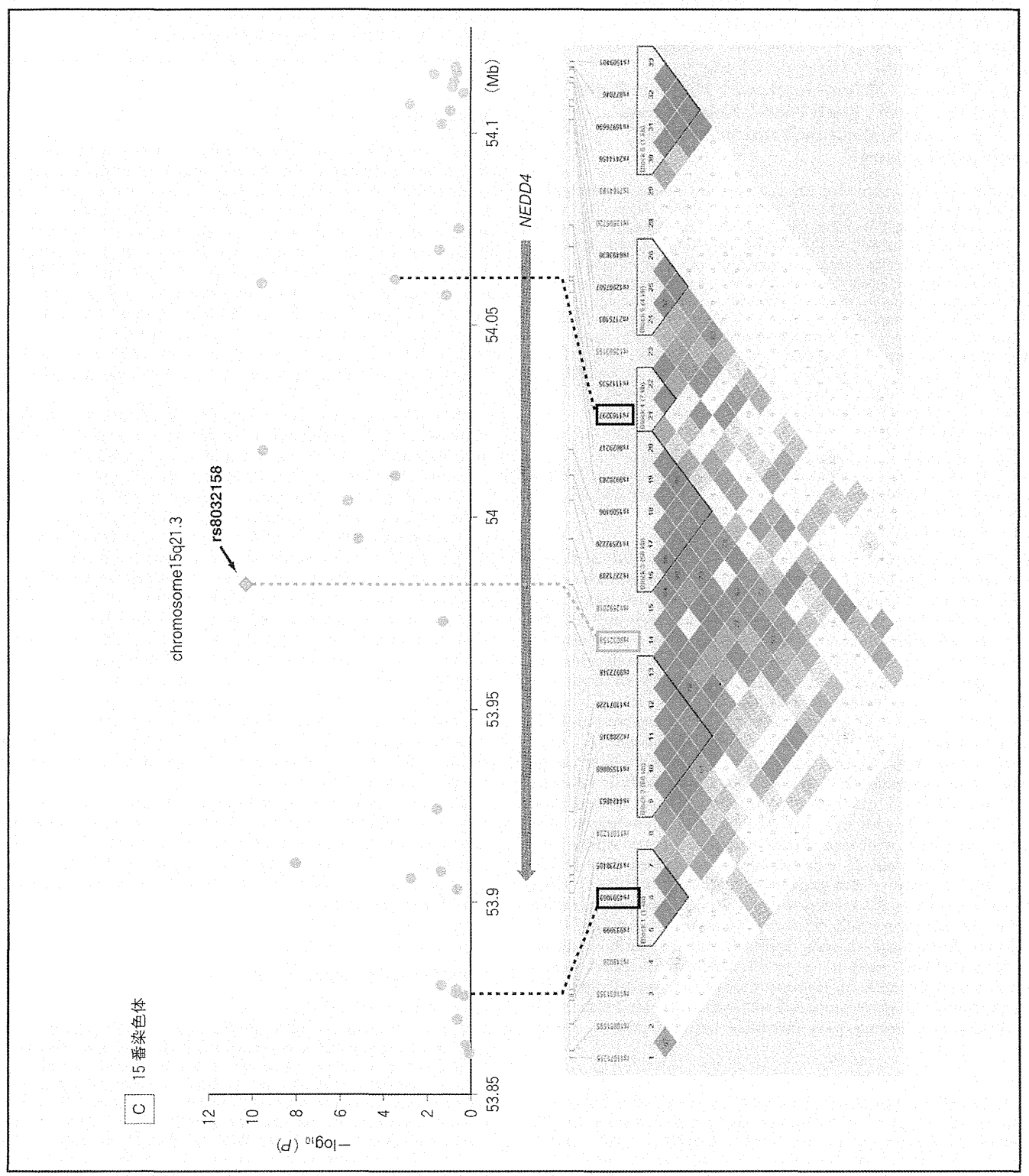

写真3　ケロイドに関連する3領域

Carcinogenesis vol.00 no.00 p.1 of 8, 2013
doi:10.1093/carcin/bgt374
Advance Access publication November 15, 2013

Association of microRNA-31 with *BRAF* mutation, colorectal cancer survival and serrated pathway

Katsuhiko Nosho[1,*,†], Hisayoshi Igarashi[1,†], Masanori Nojima[2,†], Miki Ito[1,†], Reo Maruyama[3], Shinji Yoshii[4,5], Takafumi Naito[1], Yasutaka Sukawa[1], Masashi Mikami[1], Wakana Sumioka[1], Eiichiro Yamamoto[1], Sei Kurokawa[1], Yasushi Adachi[1], Hiroaki Takahashi[1,4], Hiroyuki Okuda[1,4], Takaya Kusumi[6], Masao Hosokawa[6], Masahiro Fujita[7], Tadashi Hasegawa[8], Kenji Okita[9], Koichi Hirata[9], Hiromu Suzuki[3,†], Hiroyuki Yamamoto[10,†] and Yasuhisa Shinomura[1,†]

[1]Department of Gastroenterology, Rheumatology and Clinical Immunology, Sapporo Medical University School of Medicine, Sapporo, Japan, [2]Division of Advanced Medicine Promotion, The Advanced Clinical Research Center, The Institute of Medical Science, The University of Tokyo, Tokyo, Japan, [3]Department of Molecular Biology, Sapporo Medical University School of Medicine, Sapporo, Japan, [4]Department of Gastroenterology, Keiyukai Sapporo Hospital, Sapporo, Japan, [5]Department of Gastroenterology, NTT East Sapporo Hospital, Sapporo, Japan, [6]Department of Surgery and [7]Department of Pathology, Keiyukai Sapporo Hospital, Sapporo, Japan, [8]Department of Clinical Pathology and [9]Department of Surgery, Surgical Oncology and Science, Sapporo Medical University School of Medicine, Sapporo, Japan and [10]Division of Gastroenterology and Hepatology, Department of Internal Medicine, St. Marianna University School of Medicine, Kawasaki, Japan

*To whom correspondence should be addressed. Department of Gastroenterology, Rheumatology and Clinical Immunology, Sapporo Medical University School of Medicine, S-1, W-16, Chou-ku, Sapporo 060-8543, Japan. Tel: +81(11)611-2111; Fax: +81(11)611-2282;
Email: nosho@sapmed.ac.jp

BRAF* is an important gene in colorectal cancers (CRCs) that is associated with molecular characterization and resistance to targeted therapy. Although microRNAs (miRNAs) are useful biomarkers of various cancers, the association between miRNA and *BRAF* in CRCs is undefined. Therefore, this study was conducted to identify a relationship between specific miRNA molecules and *BRAF* mutation in CRCs and serrated lesions. miRNA array was used for the measurement of 760 miRNAs in 29 CRCs. To assess the identified miRNAs, quantitative reverse transcription–PCR was performed on 721 CRCs, 381 serrated lesions and 251 non-serrated adenomas. Moreover, proliferation and invasion assays were conducted using cell lines. miRNA array analysis revealed that microRNA-31 (miR-31)-5p was the most up-regulated miRNA in CRCs with mutated *BRAF* (*V600E*) compared with CRCs possessing wild-type *BRAF* (including cases with *KRAS* mutation). High miR-31 expression was associated with *BRAF* and *KRAS* mutations and proximal location ($P < 0.0001$). High miR-31 expression was related to cancer-specific mortality [multivariate hazard ratio = 2.06, 95% confidence interval: 1.36–3.09, $P = 0.0008$]. Functional analysis demonstrated that miR-31 inhibitor decreased cell invasion and proliferation. With regard to serrated lesions, high miR-31 expression was less frequently detected in hyperplastic polyps compared with other serrated lesions. In conclusion, associations were identified between miR-31, *BRAF* and prognosis in CRC. Transfection of miR-31 inhibitor had an antitumour effect. Thus, miR-31 may be a promising diagnostic biomarker and therapeutic target in colon cancers. Moreover, high miR-31 expression in serrated lesions suggested that miR-31 may be a key molecule in serrated pathway.

Abbreviations: CI, confidence interval; CRC, colorectal cancer; EGFR, epidermal growth factor receptor; FFPE, formalin-fixed paraffin-embedded; HP, hyperplastic polyp; HR, hazard ratio; miRNA, microRNA; miR-31, microRNA-31; MSI, microsatellite instability; MSS, microsatellite stability; OR, odds ratio; qRT–PCR, quantitative reverse transcription–PCR; SSA/P, sessile serrated adenoma/polyp; TSA, traditional serrated adenoma.

[†]These authors contributed equally to this work.

Introduction

BRAF, a member of the RAF gene family, which encodes a serine–threonine protein kinase and plays an important role in the activation of RAS–RAF–MEK–ERK signalling pathway, is one of the targeted genes in colorectal cancers (CRCs) (1–5). With regard to patient survival and chemoresistance, previous studies have shown an association between *BRAF* (*V600E*) mutation and high cancer-specific mortality rates among patients with CRC (2,5). In addition, *BRAF* has been associated with resistance to monoclonal antibodies against the epidermal growth factor receptor (EGFR) in patients with *KRAS* wild-type metastatic CRC refractory to chemotherapy (2,3). Therefore, these results suggest that further analysis of *BRAF* may enable us to identify the molecular characterization and the potential therapeutic target in CRCs.

MicroRNAs (miRNAs) constitute a class of small non-coding RNA molecules (21–25 nucleotides) that function as post-transcriptional gene regulators. miRNAs can function as oncogenes or tumour suppressors. Therefore, they have been increasingly recognized as useful biomarkers for various human cancers (6–15). In CRCs, several miRNAs are known to be deregulated (16–39) and target genes in the downstream effectors of EGFR (25,29,31–33). However, miRNAs specific to *BRAF* or its activation remain largely unknown.

The serrated pathway has attracted considerable attention as an alternative route to CRC. Approximately 30% of CRCs are hypothesized to arise from serrated lesions (40). Accumulating evidence suggests an association between CRCs with mutated *BRAF* and serrated lesions in many cases, as indicated by the high frequency of *BRAF* mutation in serrated lesions (40,41). Of these lesions, sessile serrated adenoma/polyp (SSA/P) has been identified as the precursor lesion of microsatellite instability (MSI)-high CRC with *BRAF* mutation in the proximal colon (40–42). However, the role of miRNAs in the development of CRC via the serrated pathway has not been examined in large samples of serrated lesions to date.

Therefore, we hypothesized that some specific miRNA molecules may regulate *BRAF* activation in CRCs. They may also play an important role in the progression of serrated lesions. To test this hypothesis, we conducted miRNA array analysis to detect miRNA molecules that are potentially associated with *BRAF* mutation using a database of 1353 colorectal tumours.

Materials and methods

Patients and tissue specimens

Formalin-fixed, paraffin-embedded (FFPE) tissues of 735 CRCs (stages I–IV), 391 serrated lesions and 259 non-serrated adenomas (i.e. tubular or tubulovillous adenomas) of patients who underwent endoscopic resection or other surgical treatment at Sapporo Medical University Hospital, Keiyukai Sapporo Hospital and JR Sapporo Hospital between 1997 and 2012 were collected. To avoid selection bias as far as possible, we consecutively collected FFPE specimens of CRC tissues, serrated lesions and non-serrated adenomas. The criterion for diagnosis of CRC was invasion of malignant cells beyond the muscularis mucosa. Intramucosal carcinoma and carcinoma *in situ* were classified as adenoma. Colorectal tumours were classified by location as follows: the proximal colon (caecum, ascending and transverse colon), distal colon (splenic flexure, descending and sigmoid colon) and rectum.

To clarify the association between miRNA expression and survival in metastatic CRC patients, we limited the patients who received adjuvant chemotherapy to those treated with 5-fluorouracil-based adjuvant chemotherapy. Patients with metastatic CRC treated with other targeted therapies (i.e. anti-vascular endothelial growth factor or anti-EGFR antibody) were excluded. The patients were followed up until death or December 2012, whichever came first. Informed consent was obtained from all the patients before specimen collection. This study was approved by the respective institutional review boards of the participating institutions. Tumour and paired normal colorectal tissues were reviewed by two pathologists (M.F. and T.H.). The term 'prognostic marker' is used throughout this article according to the REMARK Guidelines (43).

Histopathological evaluation of colorectal serrated lesions

Histological findings for all colorectal serrated lesion specimens were evaluated by a pathologist (M.F.) who was blinded to the clinical and molecular information. Serrated lesions [hyperplastic polyps (HPs) (N = 145), SSA/P (N = 131) and traditional serrated adenoma (TSA) (N = 115)] were classified on the basis of the current World Health Organization (WHO) criteria (44).

RNA extraction and miRNA array analysis

Total RNA was extracted from FFPE tissues using the miRNeasy FFPE Kit (Qiagen, Valencia, CA). The TaqMan® Array Human MicroRNA A + B Cards Set v3.0 (Applied Biosystems, Foster City, CA) was used for simultaneous measurement of the expression of 760 miRNAs on a microfluidic PCR platform. In brief, 1 μg of total RNA was reverse transcribed using the Megaplex Pools Kit (Applied Biosystems), following which miRNAs were amplified and detected by PCR with specific primers and TaqMan probes. PCR was run in the 7900HT Fast Real-Time PCR system (Applied Biosystems), and SDS 2.2.2 software (Applied Biosystems) was used for comparative analysis of the cycle threshold (ΔC_T). U6 snRNA (RNU6B; Applied Biosystems) served as an endogenous control. ΔC_T was calculated by subtracting the C_T values of U6 from the C_T values of the gene of interest. Expression of each miRNA in the tumour samples was calculated using the equation $2^{-\Delta C_T}$, where ΔC_T = ($C_T$miRNA – C_TU6).

Quantitative reverse transcription–PCR of miR-31

MicroRNA-31 (miR-31)-5p expression was analysed using TaqMan microRNA Assays (Applied Biosystems). In brief, 5 ng of total RNA were reverse transcribed using specific stem–loop RT primers, following which they were amplified and detected by quantitative reverse transcription–PCR (qRT–PCR) with specific primers and TaqMan probes. PCR was run in triplicate using the 7500 Fast Real-Time PCR System (Applied Biosystems). SDS v1.4 software (Applied Biosystems) was used for comparative ΔC_T analysis. U6 served as an endogenous control.

DNA extraction, pyrosequencing of KRAS, BRAF *and* PIK3CA *and MSI analysis*

Genomic DNA was extracted from FFPE tissues of colorectal tumours using QIAamp DNA FFPE Tissue Kit (Qiagen). Using extracted genomic DNA, PCR and targeted pyrosequencing were performed for *KRAS* (codons 12 and 13), *BRAF* (*V600E*) and *PIK3CA* (exons 9 and 20) (45). MSI analysis was performed using 10 microsatellite markers, as described previously (46). MSI-high was defined as instability in ≥30% of the markers, and MSI-low/microsatellite stability (MSS) as instability in <30% of the markers (46).

Sodium bisulfite treatment and pyrosequencing to measure MLH1 *promoter methylation*

Bisulfite modification of genomic DNA was performed using a BisulFlash™ DNA Modification Kit (Epigentek, Brooklyn, NY). Bisulfite pyrosequencing for *MLH1* methylation was performed using the PyroMark Kit (Qiagen), as described previously (47).

Colon cancer cell line and miRNA transient transfection

In this study, seven colon cancer cell lines (COLO-320-HSR, DLD-1, HCT-116, HT-29, Lovo, RKO and SW480) were utilized (Supplementary Table 1, available at *Carcinogenesis* Online). Total RNA was extracted from cell pellets using the TRIzol Reagent (Invitrogen by Life Technologies, Carlsbad, CA) according to the manufacturer's instructions. Cells were transfected using the Cell Line Nucleofector Kit V (Lonza, Basel, Switzerland) with a Nucleofector I electroporation device (Lonza) for DLD-1, HCT-116 and RKO and Lipofectamine 2000 (Invitrogen by Life Technologies) for COLO-320-HSR, HT-29, Lovo and SW480, according to the manufacturer's instructions. At 72 h after transfection, the cells were harvested for qRT–PCR or western blotting.

Assays for proliferation and invasion

Proliferation of miRNA transfectants was analysed by measuring the uptake of tritiated thymidine in 3-(4,5-dimethylthiazol-2-yl)-2,5-diphenyltetrazolium bromide assay (MTT assay; Sigma–Aldrich, St Louis, MO). In brief, transfected cells were seeded into 96-well plates to a density of 5×10^3 cells per well. After incubation for 0, 24, 48, 72 and 96 h, MTT assays were performed using the Cell Counting Kit-8 (Dojindo, Tokyo, Japan) according to the manufacturer's instructions.

Cell invasion was assessed by a Matrigel invasion assay. After incubation for 24 h, 1×10^6 transfected cells suspended in 500 μl of serum-free medium were added to the top of BD BioCoat Matrigel Invasion Chambers (BD Biosciences, Bedford, MA) prehydrated with phosphate-buffered saline, and 750 μl of medium supplemented with 10% fetal bovine serum was added to the lower wells of the plate. After incubation for 24 h, the invading cells were fixed, stained and analysed under a microscope (Olympus, Tokyo, Japan). Cells were counted in five random fields per membrane. In both assays, the experiments with each cell line were performed three times.

Western blot analysis

Protein expression was analysed using a standard immunoblot procedure with anti-KRAS and anti-BRAF. All primary antibodies were procured from Santa Cruz Biotechnology (Santa Cruz, CA). The anti-β-actin monoclonal antibody was used as a loading control (Oncogene Research Products, La Jolla, CA). The immunoreactive bands were visualized using enhanced chemiluminescence (Thermo Scientific, Rockford, IL).

Statistical analysis

JMP (version 10) and SAS (version 9) software programs were used for statistical analyses (SAS Institute, Cary, NC). All P values were two sided. Univariate analyses were performed to investigate clinicopathological and molecular characteristics according to the miR-31 expression level; a chi-square test or Fisher's exact test was used for categorical data, whereas analysis of variance was used to compare the mean patient age and tumour size. To account for multiple hypothesis testing in associations between miR-31 expression and other 12 covariates, the P value for significance was adjusted by Bonferroni correction to P = 0.0042 (=0.05/12).

In survival analysis, the Kaplan–Meier method and log-rank test were used to assess the survival time distribution. Cox proportional hazards regression models were used to compute mortality hazard ratios (HRs) according to the miR-31 expression status. Stratification by the tumour-node-metastasis disease stage (I, IIA, IIB, IIIA, IIIB, IIIC and IV) was performed using the 'strata' option in the SAS 'proc phreg' command. A multivariate model initially included sex (male versus female), age at diagnosis (continuous), tumour size (continuous), year of diagnosis (continuous), tumour location (proximal colon versus distal colon and rectum), tumour differentiation (well to moderate versus poor), MSI status (MSI-high versus MSS/MSI-low), *MLH1* methylation (present versus absent) and mutations of *BRAF*, *KRAS* and *PIK3CA* (present versus absent). A backward elimination was performed with a threshold of P = 0.10, to avoid overfitting. Cases with missing information for any of the categorical covariates [tumour differentiation (1.7%), MSI status (1.9%), *MLH1* methylation (4.9%), mutations of *BRAF* (0.1%), *KRAS* (1.5%) and *PIK3CA* (0.1%)] were included in the majority category of the given covariate to avoid overfitting. We confirmed that excluding cases with missing information in any of the covariates did not substantially alter results (data not shown).

A multivariate logistic regression analysis was employed to examine the associations with miR-31 expression status (as an outcome variable), adjusting for potential confounders. The model initially included a similar set of covariates to the initial Cox model. A backward elimination procedure with a threshold of P = 0.10 was used to select variables in the final model. Cases with missing information for a given covariate were included in a majority category in the initial model, and if the covariate remained in the final model, those cases were included using a missing indicator variable in the final model. The P value for significance was adjusted by Bonferroni correction to P = 0.0042 (=0.05/12).

Results

Detection of high-level miR-31 expression in BRAF*-mutated CRCs on miRNA array analysis*

To examine the miRNA expression signature in *BRAF*-mutated CRCs, 29 cases of CRCs (Supplementary Table 2, available at *Carcinogenesis* Online) were randomly selected from the CRC specimens for miRNA array analysis. Median levels of expression in the *BRAF* mutation group were compared with those in the *BRAF*

wild-type group (including cases with *KRAS* mutation). miRNA array data revealed differential expression in 33 individual miRNAs ($P < 0.05$ by Mann–Whitney *U*-test) between the two groups (Table I). All 33 miRNAs displayed higher expression levels in the *BRAF* mutation group than in the *BRAF* wild-type group. Of the 760 miRNAs, miR-31-5p was up-regulated the most often (335-fold change, $P = 0.009$).

Distribution of miR-31 expression in CRCs and association of miR-31 with clinicopathological and molecular features

We assayed miR-31 expression in 735 FFPE CRC tissue specimens and successfully obtained 721 (98%) valid results. Fourteen patients were unavailable for miR-31 expression analysis because of the lack of extracted RNA from FFPE CRC tissue specimens. We utilized 721 CRC cases, based on the availability of miR-31-5p expression data. miR-31 expression levels were quantified in CRC specimens and paired normal mucosa specimens. miR-31 expression was calculated using the equation $2^{-\Delta C_T}$, where $\Delta C_T = (C_T \text{ miR-31} - C_T \text{U6})$. To calculate the relative expression of miR-31 in each CRC, $2^{-\Delta C_T}$ of cancer tissue was divided by $2^{-\Delta C_T}$ of paired normal tissue. The distributions of miR-31 expression in the 721 CRC specimens were as follows: mean: 41.9; median: 6.3; SD: 176.2; range: 0.04–2108; interquartile range: 2.0–23.4. Cases with miR-31 expression were then divided into quartiles for further analysis: Q1 (<2.0), Q2 (2.0–6.2), Q3 (6.3–23.3) and Q4 (≥23.4). Table II shows the clinicopathological and molecular features of CRCs according to miR-31 expression level. High miR-31 expression was significantly associated with larger tumour size, proximal location, poor differentiation, advanced disease stage, *BRAF* mutation, *KRAS* mutation and MSI-high status ($P \leq 0.0042$ for all).

High miR-31 expression and patient survival

The influence of high miR-31 expression on clinical outcome was assessed in 721 CRC patients (stages I–IV). During follow-up of the 698 patients eligible for survival analysis, mortality occurred in 149, including 115 deaths confirmed to be attributable to CRCs. The median follow-up time for censored patients was 4.7 years. Kaplan–Meier analysis was performed using categorical variables (Q1, Q2, Q3 or Q4). Significantly higher mortality was observed in patients with high miR-31 expression in terms of cancer-specific survival (log-rank test: $P = 0.0013$) and overall survival (log-rank test: $P = 0.0026$) than in those with low miR-31 expression (Figure 1).

In univariate Cox regression analysis, compared with Q1 cases, significantly higher mortality rates were observed in Q2 cases [HR: 1.96; 95% confidence interval (CI): 1.06–3.77; $P = 0.031$], Q3 cases (HR: 2.16; 95% CI: 1.18–4.13; $P = 0.012$) and Q4 cases (HR: 3.10; 95% CI: 1.76–5.78; $P < 0.0001$) (Table III). Similarly, compared with Q1 cases, an independent association with shorter prognosis was observed in Q4 cases in stage-stratified (HR: 2.49; 95% CI: 1.40–4.67; $P = 0.0016$) and multivariate analyses (HR: 2.91; 95% CI: 1.60–5.57; $P = 0.0004$) for cancer-specific survival (Table III). On the other hand, compared with Q1 cases, slightly but insignificantly higher mortality rates were observed in Q2 and Q3 cases in stage-stratified (Q2: $P = 0.11$, Q3: $P = 0.23$) and multivariate stage-stratified analyses (Q2: $P = 0.14$, Q3: $P = 0.18$) (Table III). Similar results were observed in stage-stratified and multivariate stage-stratified analyses for overall survival (data not shown). Therefore, we made a dichotomous miR-31 expression variable, defining Q4 as the 'high-expression group' and combining Q1, Q2 and Q3 into the 'low-expression group'. In multivariate stage-stratified analysis, compared

Table I. Differentially expressed miRNA in *BRAF*-mutated and *BRAF* wild-type CRCs by miRNA array analysis

No.	Name of miRNA (miR base ID)	Relative miRNA expression (miRNA/U6)			*P*
		BRAF mutation group (median; $N = 7$)	*BRAF* wild-type group (median; $N = 22$)	Fold change (mutation group/wild-type group)	
1	hsa-miR-31-5p	29 925.00	89.30	335.0	0.009
2	hsa-miR-215	7.65	0.10	74.5	0.001
3	hsa-miR-151-3p	1312.00	24.40	53.8	0.003
4	hsa-miR-539-5p	370.00	7.57	48.9	0.021
5	hsa-miR-31-3p	77.30	2.14	36.1	0.002
6	hsa-miR-661	3125.00	91.80	34.1	0.011
7	hsa-miR-197-3p	4.78	0.16	29.2	0.002
8	hsa-miR-483-3p	605.00	21.90	27.6	0.032
9	hsa-miR-185-5p	15.40	0.56	27.3	0.024
10	hsa-miR-223-3p	10.50	0.40	25.9	0.005
11	hsa-miR-451a	23.50	1.00	23.5	0.015
12	hsa-miR-410	19.90	0.85	23.4	0.001
13	hsa-miR-15b-5p	9.01	0.40	22.7	0.004
14	hsa-miR-126-5p	8.45	0.37	22.6	0.013
15	hsa-miR-221-3p	99.90	4.82	20.7	0.048
16	hsa-miR-10b-3p	13.80	0.67	20.6	0.015
17	hsa-miR-29c-3p	19.50	1.02	19.1	0.001
18	hsa-miR-625-5p	185.00	10.30	18.0	0.002
19	hsa-miR-34a-5p	75.70	4.37	17.3	0.032
20	hsa-miR-7-1-3p	10.40	0.60	17.3	0.001
21	hsa-miR-10b-5p	23.10	1.49	15.5	0.008
22	hsa-miR-26b-5p	5.46	0.36	15.2	<0.001
23	hsa-let-7a-5p	5.86	0.42	13.9	0.048
24	hsa-miR-145-3p	2.82	0.20	13.8	0.028
25	hsa-miR-374a-5p	26.30	1.96	13.4	0.001
26	hsa-miR-222-3p	11.80	0.89	13.2	0.011
27	hsa-miR-379-5p	1.41	0.11	13.0	0.024
28	hsa-miR-30c-5p	1.59	0.14	11.8	0.002
29	hsa-miR-100-5p	3.26	0.28	11.6	0.004
30	hsa-miR-625-3p	13.20	1.16	11.4	0.001
31	hsa-miR-142-5p	5.23	0.48	11.0	0.002
32	hsa-miR-99a-5p	2.02	0.19	10.5	0.003
33	hsa-miR-425-5p	10.80	1.07	10.1	0.005

The fold change is expressed as the median of the *BRAF* mutation group divided by that of the wild-type group for each miRNA. *P* values were determined by the Mann–Whitney *U*-test. miRNAs with $P < 0.05$ are listed.

Table II. Clinicopathological and molecular features of 721 CRCs according to quartiles of miR-31 expression

Clinicopathological or molecular feature	Total *N*	miR-31 expression				*P*
		Q1 (<2.0)	Q2 (2.0–6.2)	Q3 (6.3–23.3)	Q4 (≥23.4)	
All cases	721	180	180	181	180	
Gender						
Male	422 (59%)	101 (56%)	107 (59%)	103 (57%)	111 (62%)	0.70
Female	299 (41%)	79 (44%)	73 (41%)	78 (43%)	69 (38%)	
Age (mean ± SD)	66.9±11.4	65.7±11.3	67.3±11.0	67.8±12.0	66.7±11.2	0.34
Tumour size (mm) (mean ± SD)	46.5±23.6	36.6±17.3	44.8±20.9	50.0±23.1	54.4±27.9	<0.0001
Year of diagnosis						
Prior to 2002	334 (46%)	93 (52%)	80 (44%)	76 (42%)	85 (47%)	0.29
2003–2012	387 (54%)	87 (48%)	100 (56%)	105 (58%)	95 (53%)	
Tumour location						
Rectum and distal colon (splenic flexure to sigmoid)	465 (64%)	135 (75%)	125 (69%)	119 (66%)	86 (48%)	<0.0001
Proximal colon (caecum to transverse)	256 (36%)	45 (25%)	55 (31%)	62 (34%)	94 (52%)	
Tumour differentiation						
Well to moderate	655 (92%)	176 (99%)	170 (96%)	162 (91%)	147 (84%)	<0.0001
Poor	54 (8.0%)	2 (1.1%)	7 (4.0%)	16 (9.0%)	29 (16%)	
Disease stage						
I	138 (19%)	59 (32%)	31 (17%)	23 (13%)	25 (14%)	<0.0001
IIA	157 (22%)	46 (26%)	42 (23%)	37 (20%)	32 (18%)	
IIB	57 (7.9%)	10 (5.6%)	10 (5.6%)	20 (11%)	17 (9.4%)	
IIIA	41 (5.7%)	14 (7.8%)	11 (6.1%)	12 (6.6%)	4 (2.2%)	
IIIB	163 (23%)	23 (13%)	45 (25%)	46 (25%)	49 (27%)	
IIIC	82 (11%)	14 (7.8%)	20 (11%)	21 (12%)	27 (15%)	
IV	83 (12%)	14 (7.8%)	21 (12%)	22 (12%)	26 (14%)	
BRAF mutation						
Wild-type	685 (95%)	176 (98%)	179 (99%)	173 (96%)	157 (87%)	<0.0001
Mutant	35 (4.9%)	3 (1.7%)	1 (0.6%)	8 (4.4%)	23 (13%)	
KRAS mutation						
Wild-type	479 (67%)	130 (74%)	123 (69%)	126 (70%)	100 (57%)	0.0042
Mutant	231 (33%)	45 (26%)	56 (31%)	54 (30%)	76 (43%)	
PIK3CA mutation						
Wild-type	642 (89%)	168 (94%)	160 (89%)	163 (90%)	151 (84%)	0.023
Mutant	78 (11%)	11 (6.2%)	20 (11%)	18 (9.9%)	29 (16%)	
MSI status						
MSS/MSI-low	658 (93%)	172 (99%)	171 (97%)	164 (92%)	151 (85%)	<0.0001
MSI-high	49 (6.9%)	2 (1.2%)	6 (3.4%)	14 (7.9%)	27 (15%)	
MLH1 methylation						
Unmethylated	387 (56%)	106 (62%)	102 (59%)	94 (54%)	85 (51%)	0.15
Methylated	299 (44%)	65 (38%)	71 (41%)	80 (46%)	83 (49%)	

Percentage (%) indicates the proportion of cases with a specific clinicopathological or molecular feature within a given quartile category (Q1, Q2, Q3 or Q4) of miR-31 expression by qRT–PCR. *P* values were calculated by analysis of variance for age and tumour size and by a chi-square test or Fisher's exact test for all other variables. To account for multiple hypothesis testing in associations between miR-31 expression and other 12 covariates, the *P* value for significance was adjusted by Bonferroni correction to $P = 0.0042$ (=0.05/12).

with the 'low-expression group', a significantly higher mortality rate was observed in the 'high-expression group' (HR: 2.06; 95% CI: 1.36–3.09; $P = 0.0008$) in cancer-specific analysis (Table III).

In stage-stratified (stages I–IV) analysis, the mortality rate in terms of cancer-specific survival was significantly higher in CRC groups (stages II–IV) with high miR-31 expression levels (log-rank test: $P = 0.035$, $P = 0.020$ and $P = 0.024$, respectively) than in those with low miR-31 expression levels (Supplementary Figure 1, available at *Carcinogenesis* Online). Our data also showed that high miR-31 expression was related to cancer-specific mortality, regardless of *BRAF* status (Supplementary Figure 2, available at *Carcinogenesis* Online).

Multivariate logistic regression analysis in cases of high miR-31 expression

Considering potential confounding and potential cause-effect sequence, we performed a multivariate logistic regression analysis to assess the relationships with miR-31 expression. The results showed that high miR-31 (Q4) expression was significantly associated with *BRAF* [odds ratio (OR): 7.05; 95% CI: 3.08–16.8; $P < 0.0001$], *KRAS* mutation (OR: 2.61; 95% CI: 1.75–3.90; $P < 0.0001$) and tumour location in the proximal colon (OR: 2.21; 95% CI: 1.49–3.28; $P < 0.0001$) (Table IV).

Association of miR-31 expression and clinicopathological and molecular features in serrated lesions

We assessed 650 FFPE tissue specimens of serrated lesions and non-serrated adenomas in the miR-31 expression assay and successfully obtained 632 (97%) valid results. Then miR-31 expression levels were also quantified in 381 colorectal serrated lesions and 251 non-serrated adenomas. It is very difficult to obtain miRNA specimens of paired normal tissue for comparison with colorectal serrated lesions and non-serrated adenomas by endoscopic resection

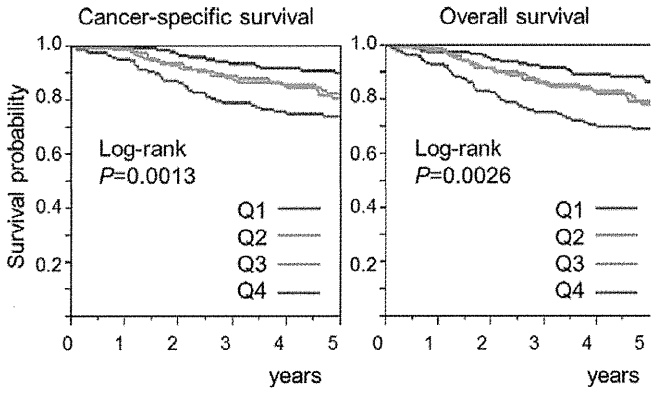

Fig. 1. Kaplan–Meier survival curves for CRCs (stages I–IV; $N = 698$) according to the miR-31 expression level. Cancer-specific survival: left panel and overall survival: right panel. Significantly higher mortality rates were observed in patients with high miR-31 expression than in those with low expression for both cancer-specific (log-rank test: $P = 0.0013$) and overall survival (log-rank test: $P = 0.0026$).

because of the small size of the resected sample. Therefore, we incorporated pooled normal mucosa specimens in each plate to standardize all assay runs. Distributions of miR-31 expression were as follows (mean ± SD; median): HP (10.3 ± 19.3; 2.6), SSA/P (20.5 ± 25.1; 12.9), TSA (24.8 ± 28.0; 14.7) and non-serrated adenoma (14.1 ± 24.9; 3.4).

Supplementary Table 3, available at *Carcinogenesis* Online, shows the clinicopathological and molecular features, including miR-31 expression, in serrated lesions and non-serrated adenomas. High miR-31 expression (Q4 in CRCs; expression level ≥23.4) was frequently detected in cases of SSA/P [32% (41/128)] and TSA [37% (42/113)] compared with those of HP [13% (18/140)] and non-serrated adenoma [19% (45/251)] ($P < 0.0001$). Multivariate regression analysis was adjusted for potential confounders including *BRAF* and *KRAS* mutations, tumour location and tumour size. The results showed a persistent significant association between high miR-31 expression and histological type [SSA/P: $P = 0.0092$, TSA: $P < 0.0001$ (HP as a referent)].

Functional analysis of miR-31 expression in colon cancer cell lines

miR-31 mimics and the inhibitor were transfected into colon cancer cell lines. The results confirmed the up-regulation or down-regulation of miR-31 expression (Supplementary Figure 3, available at *Carcinogenesis* Online). The Matrigel invasion assay revealed enhanced invasive potential of the miR-31 mimic (Figure 2A) after transfection (72 h later) into cancer cell lines. Similar results were observed in the proliferation assay (data not shown). In the proliferation assay, significantly decreased cell proliferation was also observed as a result of transfection (96 h later) of the miR-31 inhibitor (Figure 2B). Similar results were observed in the invasion assay (data not shown).

To determine the effect of miR-31 on *BRAF* and *KRAS* target proteins, expression of those proteins was compared before and after transfection (72 h later) of the miR-31 inhibitor into the cell lines. The results of western blot analysis demonstrated that after transfection, *BRAF* target proteins decreased in colon cancer cell lines, regardless of the mutational status (Figure 2C). In contrast, none of the colon cancer cell lines showed a decrease in *KRAS* target proteins.

Discussion

In this study, specific miRNA expression associated with *BRAF* (*V600E*) mutation was identified. The results of miRNA array analysis revealed that miR-31 was the most up-regulated gene in *BRAF*-mutated CRCs compared with *BRAF* wild-type CRCs. In a database of 721 patients with CRC, high miR-31 expression was associated with *BRAF* and *KRAS* mutations and proximal location in multivariate logistic regression analysis. After the transfection of the miR-31 inhibitor, western blot analysis revealed a decrease in BRAF target protein in colon cancer cell line. Thus, our data support the hypothesis

Table III. Association of miR-31 expression with patient mortality in CRCs

miR-31 expression (quartile)	Total *N*	Cancer-specific survival		
		Univariate	Stage-stratified	Multivariate stage-stratified
		HR (95% CI)	HR (95% CI)	HR (95% CI)
Q1 (<2.0)	171	1 (referent)	1 (referent)	1 (referent)
Q2 (2.0–6.2)	174	1.96 (1.06–3.77)	1.65 (0.89–3.18)	1.59 (0.86–3.07)
Q3 (6.3–23.9)	177	2.16 (1.18–4.13)	1.46 (0.79–2.81)	1.53 (0.83–2.96)
Q4 (≥24.0)	176	3.10 (1.76–5.78)	2.49 (1.40–4.67)	2.91 (1.60–5.57)
P for trend		0.0009	0.013	0.0032
Low-expression group (Q1–3)	522	1 (referent)	1 (referent)	1 (referent)
High-expression group (Q4)	176	1.84 (1.25–2.67)	1.78 (1.20–2.60)	2.06 (1.36–3.09)
P		0.0024	0.0043	0.0008

The multivariate, stage-stratified Cox model included the miR-31 expression variable stratified by sex, age at diagnosis, tumour size, year of diagnosis, tumour location, tumour differentiation, MSI status, *MLH1* methylation and mutations of *BRAF*, *KRAS* and *PIK3CA*.

Table IV. Multivariate logistic regression analysis of miR-31 expression in CRCs

Variables in the final model for miR-31 expression (as an outcome variable) [high-expression group (Q4) versus low-expression group (Q1–3)]	Adjusted OR (95% CI)	*P*
BRAF mutant (versus wild-type)	7.05 (3.08–16.8)	<0.0001
KRAS mutant (versus wild-type)	2.61 (1.75–3.90)	<0.0001
Proximal colon (versus distal colon and rectum)	2.21 (1.49–3.28)	<0.0001
Poor differentiation (versus well to moderate)	2.75 (1.38–5.44)	0.0044
Tumour size (for 30 mm increase as a unit)	1.46 (1.11–1.92)	0.0062

A multivariate logistic regression analysis assessing the relationships with miR-31 expression status initially included sex, age, tumour size, year of diagnosis, tumour location, tumour differentiation, disease stage, MSI, *MLH1* methylation, and mutations of *BRAF*, *KRAS* and *PIK3CA*, considering potential confounding and causal relationships. For multiple hypothesis testing, the *P* value for significance was adjusted by Bonferroni correction to 0.0042 (=0.05/12).

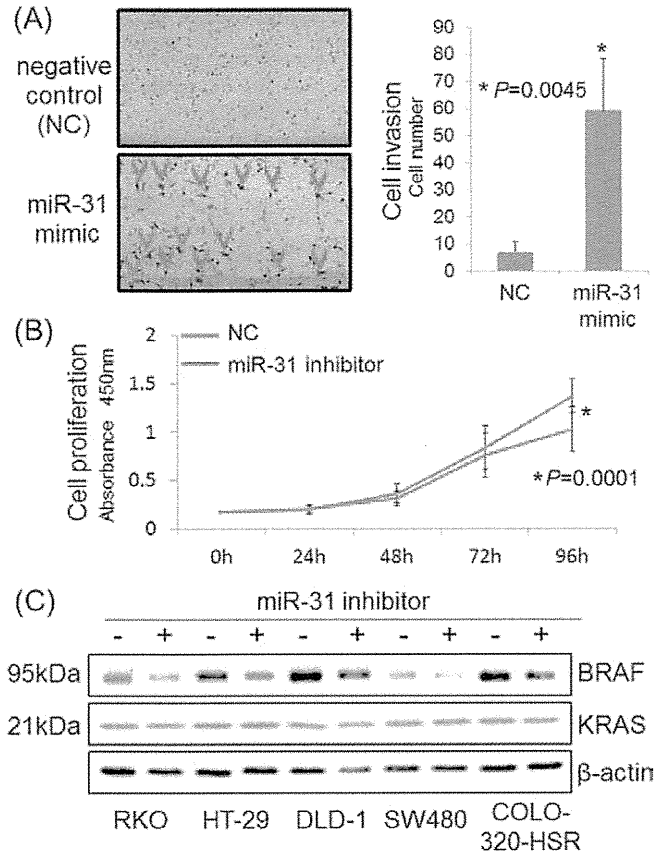

Fig. 2. Functional analysis of miR-31. (**A**) Results of the Matrigel invasion assay. Invading cells are indicated by arrow heads in the left panel. The right panel represents the means of five random microscopic fields per membrane; error bars represent the standard deviations. This assay revealed that the miR-31 mimic enhanced invasion by 8.5-fold ($P = 0.0045$) in SW480 cells (*KRAS* mutated) after transfection (72h later). The P value was analysed using a paired T-test. (**B**) In the proliferation assay, the miR-31 inhibitor significantly decreased cell proliferation in HT-29 cells (*BRAF* mutated) ($P = 0.0001$). The graph depicts the means of 16 replications; error bars represent standard deviations. (**C**) In western blot analysis, after transfection (72h later) of the miR-31 inhibitor, *BRAF* target proteins were decreased in RKO cells (*BRAF* mutated), HT-29 cells (*BRAF* mutated), DLD-1 cells (*KRAS* mutated), SW480 cells (*KRAS* mutated) and COLO-320-HSR (wild-type), respectively.

that miR-31 may regulate *BRAF* activation in CRCs. We also identified that high miR-31 expression was an unfavourable prognostic factor in patients with CRC, independent of clinicopathological and molecular features. In contrast, high miR-31 expression was frequently detected in cases with SSA/P and TSA compared with those with HP, suggesting an oncogenic role of this miRNA in the serrated pathway. The transfection of the miR-31 inhibitor exhibited an antitumour effect in functional analysis. Therefore, miR-31 may be a promising diagnostic biomarker and the therapeutic target in patients with CRC.

miR-31 is located at 9p21.3 and is reportedly deregulated in various human cancers (8,9,11,12,15). Previous studies have shown that miR-31 has oncogenic potential in oesophageal squamous cell carcinoma (8) and acts as a tumour suppressor in oesophageal adenocarcinoma (15), gastric cancer (12), ovarian cancer (11) and breast cancer (9). With regard to CRC, an association has been reported between miR-31, oncogenic potential (21–24,26,48), deeper invasion (24,48) and advanced disease stage (21,24,48); however, none of these studies have examined the association between miR-31 expression and mortality in CRC patients. In the present study, a large database was utilized. High miR-31 expression was independently associated with shorter prognosis in the multivariate stage-stratified Cox model. The importance of large-scale studies cannot be emphasized enough. Small studies with null results are much less likely to remain unpublished compared with small studies with significant results; this leads to publication bias. In contrast to previous studies (21–24,26,48), the present study examined the miR-31 expression status in a much larger sample of CRCs. Therefore, our data support the hypothesis that high miR-31 expression may be a prognostic biomarker of CRC.w Nevertheless, the data on CRCs presented here have some limitations, including the cross-sectional, observational nature of the study. Future independent studies should confirm the correlation between miR-31 and unfavourable prognosis in patients with CRC.

The tumour molecular characterization for personalized medicine is becoming important in CRCs (1–5,16,17,45). Accumulating evidence suggests that similar to *PIK3CA* and *PTEN* mutations, *BRAF* mutations confer therapeutic resistance to cetuximab and panitumumab (2,3) in patients with CRCs because these genes are located downstream of EGFR. In addition, a relationship between *BRAF* mutation and unfavourable survival has been previously reported in patients with CRCs (2,5). These results suggest that *BRAF* mutation can be a new biomarker for molecular diagnosis and identification of prognostic factors; however, no previous study has identified specific miRNAs associated with *BRAF* mutation in a large sample of colorectal tumours. In the current study, associations were identified between miR-31 expression and *BRAF* mutation and CRC prognosis. Previous studies have detected high miR-31 expression in CRC patients with MSI-high status (20,28,34) or poor differentiation (21,23). In the present study, high miR-31 expression was significantly associated with MSI-high status in univariate analysis; however, no significant association was observed in multivariate analysis. Furthermore, in serrated lesions, despite the fact that MSI-high was quite low [1.5% (6/381)], high miR-31 expression was frequently detected in cases with SSA/P and TSA. Thus, high miR-31 expression in CRC patients with MSI-high in previous studies (20,28,34) may have been due to *BRAF* mutation, which has been strongly associated with MSI-high status (1,5).

Recent studies have reported that several miRNAs target the genes in the downstream effectors of EGFR, such as miR-143 and miR-145 (25,29) for *KRAS*, miR-520a and miR-525 (30) for *PIK3CA* and miR-21 (31,32) and miR-155 (32) for *PTEN*. Moreover, *BRAF* is thought to be targeted by miR-143 and miR-145, which play a role as tumour suppressors (29). In the present study, high miR-31 expression was strongly associated with *BRAF* mutation in a CRC large sample. In addition, after transfection of the miR-31 inhibitor, western blot analysis revealed a decrease in *BRAF* target protein. These results support the hypothesis that miR-31 may regulate the activation of *BRAF* gene in CRC. The exact mechanism of this regulation by miR-31 remains unknown; however, a recent study has reported that miR-31 may target a RAS p21 GTPase-activating protein 1 (RASA1), which is a negative regulator of the RAS–RAF–MEK–ERK signalling pathway (35). Therefore, miR-31 may regulate *BRAF* activity via suppression of RASA1 in CRC, resulting in up-regulation of the signalling pathway. These findings also imply that miR-31 may serve as a molecular target of the RAF or MEK inhibitor.

Our data also showed a decrease in *BRAF* target proteins regardless of the mutational status after transfection of the miR-31 inhibitor. This decrease in *BRAF* target proteins was observed in all cell lines; however, none of the colon cancer cell lines exhibited a decrease in *KRAS* target protein. One possible explanation for these phenomena is that miR-31 may target the negative regulator, which plays a role in the pathways downstream of RAS. Further functional analysis is required to clarify the regulatory role of miR-31 in the RAS–RAF–MEK–ERK signalling pathway and its potential as a molecular target of those inhibitors.

Previously, SSA/P was often classified as HP, which was considered to have no malignant potential. However, recent studies have shown that SSA/P is mainly observed in the proximal colon (49) and is associated with frequent *BRAF* mutation and *MLH1* methylation (40–42). These results suggest that SSA/P possesses malignant potential and might be a precursor lesion of MSI-high CRC with *BRAF* mutation in the proximal colon. With regard to miRNA expression in serrated lesions, a previous study involving serrated lesions ($N = 37$) reported that SSA/P was characterized by high levels of miR-181b

and miR-21 expression compared with HP (50). However, the authors concluded that discrimination between the two lesions was impossible on the basis of miR-181b and miR-21 expression. Thus, the effects of miRNA expression in serrated lesions remain largely unknown. In the present study, high miR-31 expression was frequently detected in cases with SSA/P and TSA compared with those with HP in large samples of serrated lesions ($N = 381$). After adjusting for *BRAF* and *KRAS* mutation status, tumour location and tumour size, a persistently significant association between high miR-31 expression and the pathological features of SSA/P and TSA was observed. Thus, our data suggest that high miR-31 expression may occur in the early stage of colorectal tumorigenesis and play an oncogenic role in serrated lesions. Moreover, our findings challenge the common conception of discrete molecular features of SSA/Ps versus HPs. They may, therefore, have a substantial impact on clinical and translational research.

In conclusion, in this study, high miR-31 expression was associated with *BRAF* mutation involving a CRC large sample. This result may indicate that miR-31 is one of the important miRNAs in CRC with *BRAF* mutation. In addition, high miR-31 expression was associated with patient mortality. Finally, an antitumour effect was observed as a result of transfection of the miR-31 inhibitor. Thus, miR-31 may be a promising diagnostic biomarker and therapeutic target in patients with CRC. Moreover, our data suggest that miR-31 may play an important role in the progression of serrated lesions.

Supplementary material

Supplementary Tables 1–3 and Figures 1–3 can be found at http://carcin.oxfordjournals.org/

Funding

Japan Society for the Promotion of Science (JSPS) Grant-in-Aid for Scientific Research (23790800); A-STEP (Adaptable & Seamless Technology Transfer Program through Target-driven R&D); Daiwa Securities Health Foundation; Kobayashi Foundation for Cancer Research; Sagawa Foundation for Promotion of Cancer Research; Suzuken memorial foundation and Takeda Science Foundation.

Acknowledgements

We deeply thank the pathology departments of Sapporo Medical University Hospital, Keiyukai Sapporo Hospital and JR Sapporo Hospital for providing us with tissue specimens. The authors would like to thank Enago (www.enago.jp) for the English language review. Study concept and design: K.N.; acquisition of data: K.N., H.I., M.I., T.N., W.S., M.F. and T.H.; analysis and interpretation of data: K.N., H.I., R.M.M.N., H.S., H.Y. and Y.S.; drafting of the manuscript: K.N., H.I., M.I. and H.Y.; critical revision of the manuscript for important intellectual content: K.N., H.I., M.I., R.M., Y.S., E.Y., S.K. and Y.S.; statistical analysis: K.N. and M.N.; material support: S.Y., M.M., H.T., H.O., T.K., M.H., M.F., T.H., K.O. and K.H.: study supervision: H.S., H.Y. and Y.S.; final approval of manuscript: all authors.

Conflict of Interest Statement: None declared.

References

1. Network,T.C.G.A. (2012) Comprehensive molecular characterization of human colon and rectal cancer. *Nature*, **487**, 330–337.
2. De Roock,W. *et al.* (2011) KRAS, BRAF, PIK3CA, and PTEN mutations: implications for targeted therapies in metastatic colorectal cancer. *Lancet Oncol.*, **12**, 594–603.
3. Di Nicolantonio,F. *et al.* (2008) Wild-type BRAF is required for response to panitumumab or cetuximab in metastatic colorectal cancer. *J. Clin. Oncol.*, **26**, 5705–5712.
4. Donehower,L.A. *et al.* (2013) MLH1-silenced and non-silenced subgroups of hypermutated colorectal carcinomas have distinct mutational landscapes. *J. Pathol.*, **229**, 99–110.
5. Lochhead,P. *et al.* (2013) Microsatellite instability and BRAF mutation testing in colorectal cancer prognostication. *J. Natl. Cancer Inst*, **105**, 1151–1156.
6. Nishikawa,E. *et al.* (2011) miR-375 is activated by ASH1 and inhibits YAP1 in a lineage-dependent manner in lung cancer. *Cancer Res.*, **71**, 6165–6173.
7. Lu,J. *et al.* (2005) MicroRNA expression profiles classify human cancers. *Nature*, **435**, 834–838.
8. Zhang,T. *et al.* (2011) The oncogenetic role of microRNA-31 as a potential biomarker in oesophageal squamous cell carcinoma. *Clin. Sci. (Lond).*, **121**, 437–447.
9. Valastyan,S. *et al.* (2009) A pleiotropically acting microRNA, miR-31, inhibits breast cancer metastasis. *Cell*, **137**, 1032–1046.
10. Meng,F. *et al.* (2007) MicroRNA-21 regulates expression of the PTEN tumor suppressor gene in human hepatocellular cancer. *Gastroenterology*, **133**, 647–658.
11. Creighton,C.J. *et al.* (2010) Molecular profiling uncovers a p53-associated role for microRNA-31 in inhibiting the proliferation of serous ovarian carcinomas and other cancers. *Cancer Res.*, **70**, 1906–1915.
12. Zhang,Y. *et al.* (2010) Down-regulation of miR-31 expression in gastric cancer tissues and its clinical significance. *Med. Oncol.*, **27**, 685–689.
13. Schaefer,A. *et al.* (2010) Diagnostic and prognostic implications of microRNA profiling in prostate carcinoma. *Int. J. Cancer*, **126**, 1166–1176.
14. Ueda,T. *et al.* (2010) Relation between microRNA expression and progression and prognosis of gastric cancer: a microRNA expression analysis. *Lancet Oncol.*, **11**, 136–146.
15. Leidner,R.S. *et al.* (2012) The microRNAs, MiR-31 and MiR-375, as candidate markers in Barrett's esophageal carcinogenesis. *Genes. Chromosomes Cancer*, **51**, 473–479.
16. Bartley,A.N. *et al.* (2011) Complex patterns of altered MicroRNA expression during the adenoma-adenocarcinoma sequence for microsatellite-stable colorectal cancer. *Clin. Cancer Res.*, **17**, 7283–7293.
17. Balaguer,F. *et al.* (2011) Colorectal cancers with microsatellite instability display unique miRNA profiles. *Clin. Cancer Res.*, **17**, 6239–6249.
18. Schetter,A.J. *et al.* (2008) MicroRNA expression profiles associated with prognosis and therapeutic outcome in colon adenocarcinoma. *JAMA*, **299**, 425–436.
19. Shibuya,H. *et al.* (2010) Clinicopathological and prognostic value of microRNA-21 and microRNA-155 in colorectal cancer. *Oncology*, **79**, 313–320.
20. Sarver,A.L. *et al.* (2009) Human colon cancer profiles show differential microRNA expression depending on mismatch repair status and are characteristic of undifferentiated proliferative states. *BMC Cancer*, **9**, 401.
21. Schee,K. *et al.* (2012) Clinical relevance of microRNA miR-21, miR-31, miR-92a, miR-101, miR-106a and miR-145 in colorectal cancer. *BMC Cancer*, **12**, 505.
22. Cekaite,L. *et al.* (2012) MiR-9, -31, and -182 deregulation promote proliferation and tumor cell survival in colon cancer. *Neoplasia*, **14**, 868–879.
23. Chang,K.H. *et al.* (2011) MicroRNA signature analysis in colorectal cancer: identification of expression profiles in stage II tumors associated with aggressive disease. *Int. J. Colorectal Dis.*, **26**, 1415–1422.
24. Wang,C.J. *et al.* (2009) Clinicopathological significance of microRNA-31, -143 and -145 expression in colorectal cancer. *Dis. Markers*, **26**, 27–34.
25. Chen,X. *et al.* (2009) Role of miR-143 targeting KRAS in colorectal tumorigenesis. *Oncogene*, **28**, 1385–1392.
26. Slaby,O. *et al.* (2007) Altered expression of miR-21, miR-31, miR-143 and miR-145 is related to clinicopathologic features of colorectal cancer. *Oncology*, **72**, 397–402.
27. Bandrés,E. *et al.* (2006) Identification by Real-time PCR of 13 mature microRNAs differentially expressed in colorectal cancer and non-tumoral tissues. *Mol. Cancer*, **5**, 29.
28. Earle,J.S. *et al.* (2010) Association of microRNA expression with microsatellite instability status in colorectal adenocarcinoma. *J. Mol. Diagn.*, **12**, 433–440.
29. Pagliuca,A. *et al.* (2013) Analysis of the combined action of miR-143 and miR-145 on oncogenic pathways in colorectal cancer cells reveals a coordinate program of gene repression. *Oncogene*, **32**, 4806–4813.
30. Arcaroli,J.J. *et al.* (2012) Common PIK3CA mutants and a novel 3' UTR mutation are associated with increased sensitivity to saracatinib. *Clin. Cancer Res.*, **18**, 2704–2714.
31. Xiong,B. *et al.* (2013) MiR-21 regulates biological behavior through the PTEN/PI-3 K/Akt signaling pathway in human colorectal cancer cells. *Int. J. Oncol.*, **42**, 219–228.
32. Bakirtzi,K. *et al.* (2011) Neurotensin signaling activates microRNAs-21 and -155 and Akt, promotes tumor growth in mice, and is increased in human colon tumors. *Gastroenterology*, **141**, 1749–61.e1.

33. Mosakhani,N. *et al.* (2012) MicroRNA profiling differentiates colorectal cancer according to KRAS status. *Genes. Chromosomes Cancer*, **51**, 1–9.
34. Oberg,A.L. *et al.* (2011) miRNA expression in colon polyps provides evidence for a multihit model of colon cancer. *PLoS One*, **6**, e20465.
35. Sun,D. *et al.* (2013) MicroRNA-31 activates the RAS pathway and functions as an oncogenic MicroRNA in human colorectal cancer by repressing RAS p21 GTPase activating protein 1 (RASA1). *J. Biol. Chem.*, **288**, 9508–9518.
36. Hur,K. *et al.* (2013) MicroRNA-200c modulates epithelial-to-mesenchymal transition (EMT) in human colorectal cancer metastasis. *Gut*, **62**, 1315–1326.
37. Takahashi,M. *et al.* (2012) Boswellic acid exerts antitumor effects in colorectal cancer cells by modulating expression of the let-7 and miR-200 microRNA family. *Carcinogenesis*, **33**, 2441–2449.
38. Wu,J. *et al.* (2012) MicroRNA-34a inhibits migration and invasion of colon cancer cells via targeting to Fra-1. *Carcinogenesis*, **33**, 519–528.
39. Yu,Y. *et al.* (2012) MicroRNA-21 induces stemness by downregulating transforming growth factor beta receptor 2 (TGFβR2) in colon cancer cells. *Carcinogenesis*, **33**, 68–76.
40. Bettington,M. *et al.* (2013) The serrated pathway to colorectal carcinoma: current concepts and challenges. *Histopathology*, **62**, 367–386.
41. Leggett,B. *et al.* (2010) Role of the serrated pathway in colorectal cancer pathogenesis. *Gastroenterology*, **138**, 2088–2100.
42. Rosty,C. *et al.* (2012) Phenotype and polyp landscape in serrated polyposis syndrome: a series of 100 patients from genetics clinics. *Am. J. Surg. Pathol.*, **36**, 876–882.
43. McShane,L.M. *et al.*; Statistics Subcommittee of the NCI-EORTC Working Group on Cancer Diagnostics. (2005) Reporting recommendations for tumor marker prognostic studies (REMARK). *J. Natl. Cancer Inst.*, **97**, 1180–1184.
44. Bosman,F.T. *et al.* (2010) *WHO Classification of Tumours of the Digestive System*. International Agency for Research on Cancer, Lyon, France.
45. Liao,X. *et al.* (2012) Aspirin use, tumor PIK3CA mutation, and colorectal-cancer survival. *N. Engl. J. Med.*, **367**, 1596–1606.
46. Nosho,K. *et al.* (2009) A prospective cohort study shows unique epigenetic, genetic, and prognostic features of synchronous colorectal cancers. *Gastroenterology*, **137**, 1609–20.e1.
47. Iwagami,S. *et al.* (2013) LINE-1 hypomethylation is associated with a poor prognosis among patients with curatively resected esophageal squamous cell carcinoma. *Ann. Surg.*, **257**, 449–455.
48. Cottonham,C.L. *et al.* (2010) miR-21 and miR-31 converge on TIAM1 to regulate migration and invasion of colon carcinoma cells. *J. Biol. Chem.*, **285**, 35293–35302.
49. Torlakovic,E.E. *et al.* (2008) Sessile serrated adenoma (SSA) vs. traditional serrated adenoma (TSA). *Am. J. Surg. Pathol.*, **32**, 21–29.
50. Schmitz,K.J. *et al* (2009) Differential expression of microRNA 181b and microRNA 21 in hyperplastic polyps and sessile serrated adenomas of the colon. *Virchows Arch.*, **455**, 49–54.

Received September, 4, 2013; revised October 16, 2013; accepted November 9, 2013

Hepatic biliary epithelial cells acquire epithelial integrity but lose plasticity to differentiate into hepatocytes *in vitro* during development

Naoki Tanimizu[1,*], Yukio Nakamura[2], Norihisa Ichinohe[1], Toru Mizuguchi[2], Koichi Hirata[2] and Toshihiro Mitaka[1]

[1]Department of Tissue Development and Regeneration, Research Institute for Frontier Medicine, Sapporo Medical University School of Medicine, S-1, W-17, Chuo-ku, Sapporo, Japan
[2]First Department of Surgery, Sapporo Medical University School of Medicine, Sapporo Medical University School of Medicine, S-1, W-17, Chuo-ku, Sapporo, Japan
*Author for correspondence (tanimizu@sapmed.ac.jp)

Accepted 4 September 2013
Journal of Cell Science 126, 5239 5246

doi: 10.1242/jcs.133082

Summary

In developing organs, epithelial tissue structures are mostly developed by the perinatal period. However, it is unknown whether epithelial cells are already functionally mature and whether they are fixed in their lineage. Here we show that epithelial cells alter their plasticity during postnatal development by examining the differentiation potential of epithelial cell adhesion molecule $(EpCAM)^+$ cholangiocytes (biliary epithelial cells) isolated from neonatal and adult mouse livers. We found that neonatal cholangiocytes isolated from 1 week old liver converted into functional hepatocytes in the presence of oncostatin M and Matrigel®. In contrast, neither morphological changes nor expression of hepatocyte markers were induced in adult cholangiocytes. The transcription factors hepatocyte nuclear factor 4α and CCAAT/enhancer binding protein α (C/EBPα), which are necessary for hepatocytic differentiation, were induced in neonatal cholangiocytes but not in adult cells, whereas grainyhead like 2 (Grhl2) and hairy enhance of slit 1 (Hes1), which are implicated in cholangiocyte differentiation, were continuously expressed in adult cells. Overexpression of C/EBPα and Grhl2 promoted and inhibited hepatocytic differentiation, respectively. Furthermore, adult cholangiocytes formed a monolayer with higher barrier function than neonatal ones did, suggesting that cholangiocytes are still in the process of epithelial maturation even after forming tubular structures during the neonatal period. Taken together, these results suggest that cholangiocytes lose plasticity to convert into hepatocytes during epithelial maturation. They lose competency to upregulate hepatocytic transcription factors and downregulate cholagiocytic ones under conditions inducing hepatocytic differentiation. Our results suggest that a molecular machinery augmenting epithelial integrity limits lineage plasticity of epithelial cells.

Key words: Epithelial progenitors, Plasticity, Cholangiocytes, Bile duct, Mature hepatocytes

Introduction

During development, tissue stem/progenitor cells differentiate to multiple types of epithelial cells, which establish various tissue structures, including alveoli in the lung, renal tubules in the kidney, and hepatic cords and bile ducts in the liver. Given that organs need to perform their physiological functions after the birth, epithelial tissue structures may be mostly developed at the birth or soon after. However, it is unknown whether epithelial cells are fixed in their lineage and fully functional in neonatal organs.

The liver contains two types of epithelial cells, named hepatocytes and cholangiocytes, which originate from hepatoblasts (fetal liver stem/progenitor cells) during development (Oertel et al., 2003; Tanimizu et al., 2003). Cholangiocytes are biliary epithelial cells forming bile duct tubules. Bile ducts connect the liver to the intestine to drain the bile secreted by hepatocytes. It can be assumed that cholangiocytes acquire epithelial characteristics including secretory and barrier functions when they establish the tubular structure, since it is physiologically important to modulate the composition of bile and avoid any leakage of bile during drainage. However, it is unknown whether cholangiocytes in the neonatal liver have similar epithelial characteristics as those in the adult liver.

In the adult liver, there are at least three possible sources of hepatocytes and cholangiocytes: self duplication of mature cells, the stem cell system, and lineage conversion. The self duplication of hepatocytes and cholangiocytes to replace aged or damaged cells is the simplest way, which may be the case in normal and in acutely injured livers (Michalopoulos, 2007; Malato et al., 2011). In contrast, after severe chronic liver injury, the duplication ability of the epithelial cells may be exhausted and stem or progenitor cells may be activated to supply hepatocytes and cholangiocytes (Espanol Suner et al., 2012). In addition to the self duplication and stem/progenitor cell systems, lineage conversion should be taken into consideration (Michalopoulos, 2011). It has been shown that mature hepatocytes (MHs) have the potential to transdifferentiate into cholangiocyte like cells (Nishikawa et al., 2005; Zong et al., 2009). In contrast to hepatocytes, it remains unclear whether cholangiocytes have the ability to convert into hepatocytes.

In this work we examined the differentiation potential of cholangiocytes in neonatal and adult mouse liver. We found that neonatal, but not adult, epithelial cell adhesion molecule $(EpCAM)^+$ cholangiocytes expressed hepatocytic transcription factors and converted into hepatocytes *in vitro* that were structurally and functionally similar to MHs. Interestingly, neonatal cholangiocytes are still immature compared with adult ones even though they have already established tubular structures *in vivo*. Our results indicate that neonatal cholangiocytes possess plasticity to convert into hepatocytes but lose this ability during maturation of bile ducts. We further demonstrated that a transcription factor implicated in epithelial maturation limited lineage plasticity of cholangiocytes.

Results

Cholangiocytes proliferate and retain the cholangiocytic phenotype on type I collagen gel

Because the number of cholangiocytes isolated from the liver is limited and not enough to examine their differentiation potential, we first established a primary culture in which cholangiocytes keep the original characteristics and efficiently proliferate. To isolate mature cholangiocytes from 6 week old (6W) mouse liver, two step collagenase perfusion was performed and the remaining tissue containing Glisson's capsules was further digested. $EpCAM^+$ cholangiocytes were enriched by magnetic activated cell sorting (MACS; supplementary material Fig. S1). They were plated on culture wells coated with type I collagen (Col I) or a thin layer of Matrigel (MG), or covered with Col I gel or MG gel (Fig. 1A). On wells coated with Col I, only a very small number of cells survived and proliferated. On MG coated or MG gel wells, 2 or 3 days after plating, cells began to proliferate slowly. On Col I gel, cells proliferated very efficiently. In all four conditions, cells survived and proliferated after replating at day 7 of primary culture. Importantly, on Col I gel, as well as MG gel, expression of EpCAM was retained on cholangiocytes but disappeared when grown in wells coated with Col I (Fig. 1B; supplementary material Fig. S2). During the culture on Col I gel, cholangiocytes maintained expression of cholangiocyte markers [osteopontin (OPN), SRY related HMG box transcription factor 9 (Sox9) and hepatocyte nuclear factor (Hnf)1β], but did not express the hepatocyte marker, Hnf4α (Fig. 1C), and kept epithelial characteristics, such as the ability to form cystic structures in 3D culture; about 1% of cells formed cysts during 10 days in culture ever after the fourth passage (Fig. 1D; supplementary material Fig. S2). We further confirmed that, like mouse cholangiocytes, human $EpCAM^+$ cholangiocytes proliferated and retained the expression of EpCAM on Col I gel (supplementary material Fig. S3). In the following experiments, we examined differentiation potential of cholangiocytes after expansion in Col I gel culture.

Hepatocytic differentiation potential of adult cholangiocytes

To examine the hepatocytic differentiation potential of cholangiocytes, $EpCAM^+$ cells derived from 6 8W mouse livers were cultured on Col I gel for 5 days and then replated onto dishes coated with gelatin. To induce hepatocytic differentiation, oncostatin M (OSM) was added to the culture medium after the cells reached confluency. On day 9 in culture,

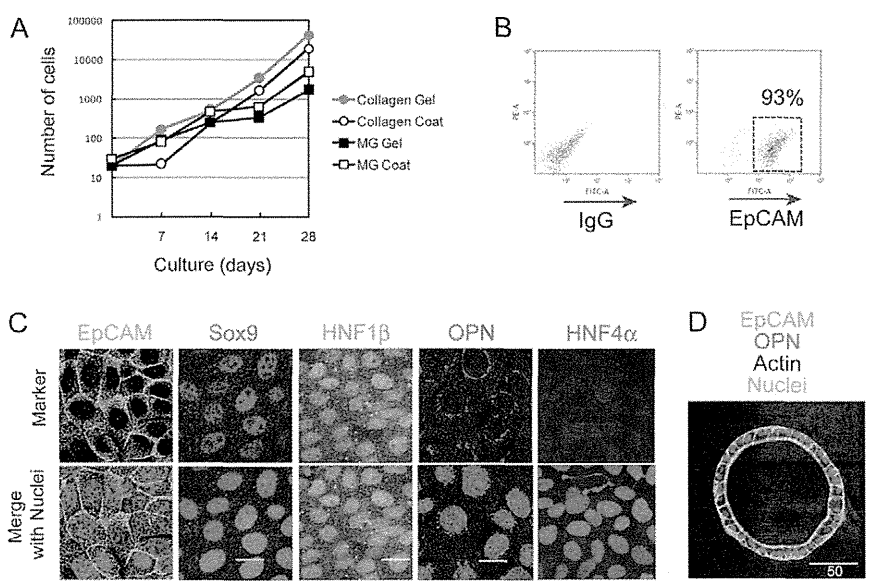

Fig. 1. *In vitro* expansion of $EpCAM^+$ cholangiocytes on Col-I gel. (A) Proliferation of $EpCAM^+$ cholangiocytes on Col-I and Matrigel®. Cholangiocytes were cultured on Col-I-coated or MG-coated wells or on Col-I gel or MG. Every 7 days, they were replated onto dishes coated with the same extracellular matrix as the primary culture. During primary culture, cholangiocytes proliferated on Col-I gel, MG gel and MG-coated dishes, though they proliferated most efficiently on Col-I gel. Beyond secondary culture, cholangiocytes proliferated in all conditions. (B) Adult cholangiocytes retained the expression of EpCAM on Col-I gel. EpCAM expression was examined by fluorescence-activated cell sorting (FACS). More than 90% of cells retained EpCAM expression on Col-I gel. (C) Adult cholangiocytes retained the expression of marker genes on Col-I gel. Cultured cholangiocytes expressed the cholangiocyte markers EpCAM, Sox9, HNF1β, and OPN. $EpCAM^+$ cells isolated from 6W mouse liver were cultured on Col-I gel for 7 days, fixed in 4% PFA, and incubated with anti-Sox9, anti-HNF1β and anti-OPN antibodies. Nuclei were counterstained with Hoechst 33258. (D) Adult cholangiocytes form cysts with the central lumen in three-dimensional culture. At day 7, cultured cholangiocytes were dissociated from Col-I gel, replated on a layer of MG, and then overlaid with 5% MG. Cysts were stained with anti-EpCAM (green), anti-OPN (red), and phalloidin (white). Nuclei were counterstained with Hoechst33258 (blue).

cells were overlaid with 5% MG (Fig. 2A). Dense cytoplasm and clear cell cell contacts were observed after sequential treatment with OSM and MG (Fig. 2B). However, as shown in Fig. 2B, the cells barely expressed hepatocyte markers including albumin, carbamoylphosphate synthetase I (CPSI), phosphoenolpyruvate carboxykinase (PEPCK), and tryptophan 2,3 dioxygenase (Tdo2). Thus, hepatocytic characteristics could not be induced in adult cholangiocytes.

Hepatocytic differentiation potential of neonatal cholangiocytes

To investigate whether cholangiocytes have the potential to differentiate into hepatocytes during the early stage of bile duct formation, we applied the same culture conditions to neonatal cholangiocytes isolated from 1W liver. Similar to adult cholangiocytes, neonatal cholangiocytes continued to express cholangiocyte markers during culture on Col I gel (supplementary material Fig. S4). As shown in Fig. 2A, neonatal cells cultured on gelatin proliferated and formed a monolayer in which the cells were in close contact with each other. After addition of OSM to the medium on day 5, the cells altered their morphology, developing round nuclei and dense cytoplasm. When the cells were overlaid with MG, cytoplasmic granularity increased. Furthermore, bile canaliculus (BC) like structures were observed between the cells. During the sequential treatment of OSM and MG, there was increased expression of the genes for albumin, metabolic enzymes including glucose 6 phosphatase (G6Pase), PEPCK, tyrosine aminotransferase (TAT), Tdo2, CPSI and cytochrome P450 proteins (Cyps) (Fig. 2B). We also examined expression of cholangiocyte markers including cytokeratin (CK) 7, CK19 and EpCAM, and found that CK7 and EpCAM were downregulated during hepatocytic differentiation (Fig. 2B and supplementary material Fig. S5). Immunocytochemical analysis showed that albumin and CPSI proteins, which were not expressed in neonatal cholangiocytes at the beginning of the culture period, were expressed in the cytoplasm after inducing hepatocytic differentiation (Fig. 2C3; Figs 4, 7, 8), whereas both proteins were not induced in adult cholangiocytes (Fig. 2C1; Figs 2, 5, 6). However, EpCAM was not downregulated in adult cholangiocytes but was in neonatal ones during culture (Fig. 2C9 12). To examine whether cells treated with MG acquired differentiated functions, ammonium chloride was added to the culture medium. The concentration of ammonium ions in the medium gradually decreased with the time in the wells of cultured neonatal cholangiocytes but not in those of adult cells

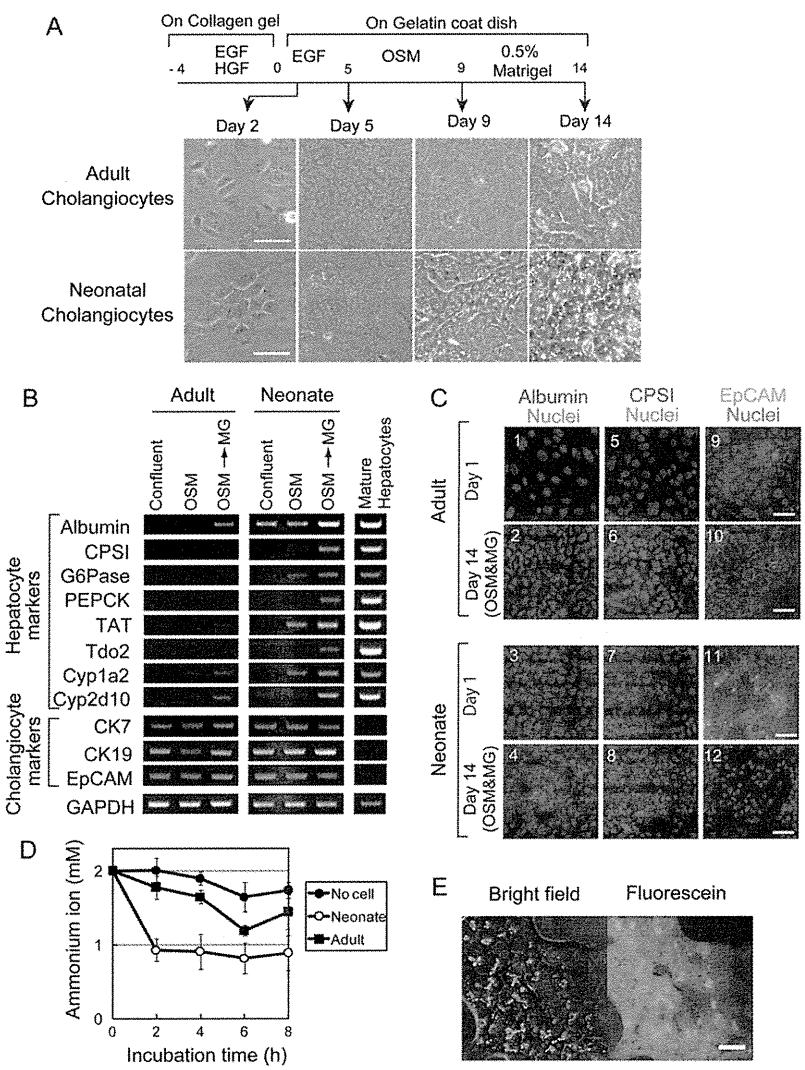

Fig. 2. Neonatal, but not adult, cholangiocytes differentiate to functional hepatocytes. (A) Morphological changes of adult and neonatal cholangiocytes during culture. Adult cholangiocytes show dense cytoplasm at day 5 in culture. Cell cell contacts were clearly visible after overlaying with MG. Neonatal cholangiocytes had round nuclei and dense cytoplasm in the presence of OSM. Cell cell contacts were more evident after overlaying with MG. After expansion on Col-I gel, adult and neonatal cholangiocytes were used to induce hepatocytic characteristics by sequentially treating them with OSM and MG. Scale bars: 50 μm. (B) Neonatal cholangiocytes were induced to express hepatocyte markers. Hepatocyte marker expression was examined by PCR. Adult cholangiocytes weakly expressed albumin but not other hepatocyte markers even in the presence of OSM and MG. In contrast, hepatocyte markers such as CPSI, G6Pase, PEPCK, TAT and Tdo2 were induced in neonatal cholangiocytes during culture. Cyp1a2 and Cyp2d10 were also expressed. Among cholangiocyte markers, CK7 and EpCAM were slightly downregulated in the presence of OSM and MG. Experiments were repeated three times, independently, and the representative data are shown. (C) Expression of hepatocyte markers at the protein level. At 1 day after plating onto gelatin-coated dishes, neonatal cholangiocytes did not express albumin and CPSI. After inducing hepatocytic differentiation, albumin (red) was expressed in many cells. Some cells expressed CPSI (red). In contrast, both proteins were not expressed in adult cholangiocytes before and after treatment of OSM and MG. Scale bars: 50 μm. (D) Hepatocytes derived from neonatal cholangiocytes eliminated ammonium ions from the medium. Ammonium chloride (2 mM) was added to neonatal cholangiocytes treated with MG. Ammonium ions in the medium were eliminated by hepatocytes derived from neonatal cholangiocytes. Average values at each time point are shown (±s.d.). (E) Hepatocytes derived from neonatal EpCAM^{+} cells formed BC-like structures. After incubation in the presence of MG, cells were further treated with 100 μM taurocholate, and FDA was then added. Hepatocytes derived from neonatal cholangiocytes metabolized FDA and fluorescein was secreted into BC-like structures. Scale bar: 50 μm.

(Fig. 2D). Finally, to confirm whether BC like structures were generated, we added fluorescein diacetate (FDA) to the culture medium after augmenting formation of BC like structures in the presence of taurocholate (Fu et al., 2011). We found that metabolized fluorescein was excreted into BC like structures (Fig. 2E). These data indicate that cholangiocytes possessed the ability to convert into functional hepatocytes during the neonatal period.

HNF4α and C/EBPα are induced in neonatal cholangiocytes during culture

Transcription factors have been shown to determine and convert the lineages of many types of cells. At the time when hepatoblasts are committed to cholangiocytes, transcription factors related to hepatocytic differentiation, including HNF4α and CCAAT/enhancer binding protein α (C/EBPα), are suppressed, whereas those related to cholangiocytic differentiation are upregulated (Tanimizu and Miyajima, 2004; Yamasaki et al., 2006). Therefore, we tested the possibility that the expression patterns of these transcription factors differ between neonatal and mature cholangiocytes. We focused on HNF4α and C/EBPα, because both of these are crucial for the differentiation and/or maturation of hepatocytes (Parviz et al., 2003; Mackey and Darlington, 2004). Using quantitative PCR, we examined the expression of *HNF4α* and *C/EBPα* in neonatal and mature cholangiocytes during culture for hepatocytic differentiation. We also examined the expression of *FoxA1* (*HNF3α*), which has been shown to be a crucial factor conferring hepatocytic characteristics on multipotent as well as somatic cells (Sekiya et al., 2009; Sekiya and Suzuki, 2011). HNF4α and C/EBPα genes were clearly induced in neonatal but not in mature cholangiocytes, whereas *FoxA1* was expressed in both cell types (Fig. 3A). These results suggest that the efficient induction of HNF4α and C/EBPα is necessary for cholangiocytes to convert into hepatocytes. Immunofluorescence analysis further confirmed that HNF4α and C/EBPα were induced in neonatal cholangiocytes but not in adult ones after inducing hepatocytic differentiation (Fig. 3B).

Overexpression of C/EBPα and inhibition of the Notch signaling pathway slightly increase hepatocyte gene expression in mature cholangiocytes

To examine whether HNF4α and C/EBPα could induce hepatocytic characteristics, we introduced their cDNAs into mature cholangiocytes using retroviral vectors. Cholangiocytes induced with HNF4α or C/EBPα were sequentially treated with OSM and MG. Both HNF4α and C/EBPα slightly increased expression of albumin, whereas only C/EBPα upregulated *CPSI* (Fig. 3C).

Because the Notch signaling pathway has been implicated in cholangiocyte differentiation of hepatoblasts and hepatocytes (Tanimizu and Miyajima, 2004; Zong et al., 2009), we considered a possibility that constitutive activation of the pathway might inhibit hepatocytic differentiation of adult cholangiocytes. Therefore, we also examined whether inhibition of the Notch pathway by adding 3,5 difluorophenylacetyl L alanyl L 2 phenylglycine *t* butyl ester (DAPT), a γ secretase inhibitor that potentially blocks the Notch signaling pathway (Sastre et al., 2001), could induce the hepatocytic differentiation of mature cholangiocytes. The DAPT treatment slightly decreased expression of *Hes1*, one of major targets of the

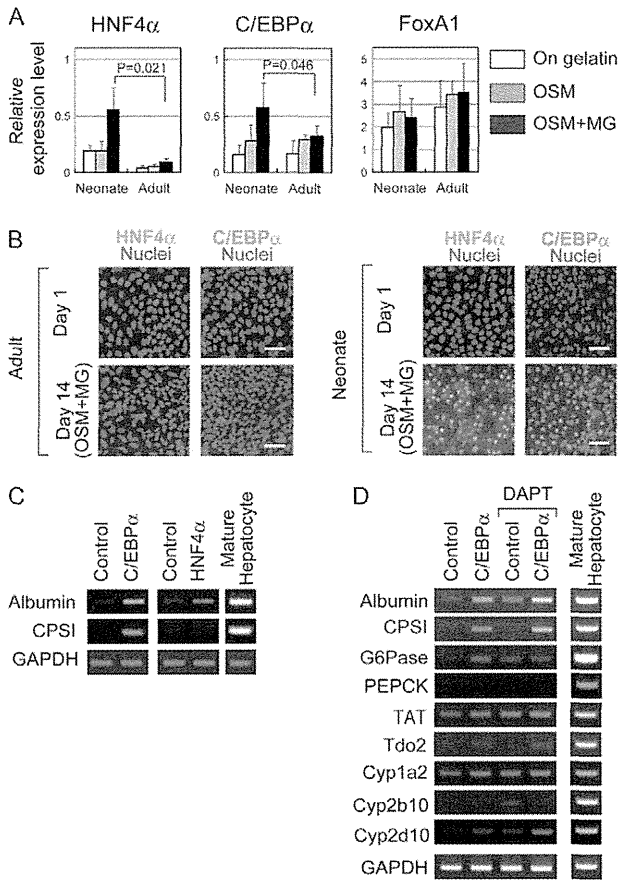

Fig. 3. Overexpression of C/EBPα slightly induces CPSI expression in adult cholangiocytes. (A) Expression of HNF4α, C/EBPα and FoxA1 in cholangiocytes during culture. HNF4α and C/EBPα were induced in neonatal cholangiocytes but not in adult cholangiocytes. FoxA1 was expressed in both types of cells. Expression levels are presented relative to the expression levels in MHs cultured for 1 day. Two-tailed Student's *t*-tests were performed using Microsoft Excel. (B) Protein expression of HNF4α and CPSI. HNF4α and C/EBPα proteins were induced in neonatal cholangiocytes after inducing hepatocytic differentiation. Nuclei were counterstained with Hoechst 33258. Scale bars: 50 μm. (C) Expression of CPSI was induced by the overexpression of C/EBPα, but not HNF4α. (D) Induction of hepatocyte markers by overexpression of C/EBPα in the presence of a γ-secretase inhibitor. Expression of albumin and CPSI hepatocytic induced by C/EBPα was further upregulated in the presence of DAPT, a γ-secretase inhibitor and a potent inhibitor for the Notch signaling pathway. The data also show that expression of Tdo2 and Cyp2d10 were slightly increased.

Notch pathway, whereas expression of albumin was significantly increased in the presence of DAPT (supplementary material Fig. S6).

Next, we examined whether overexpression of C/EBPα and inhibition of the Notch pathway have an additive effect on hepatocytic differentiation. As shown in Fig. 3D, albumin and *CPSI* were induced to a greater extent by a combination of DAPT and C/EBPα expression than by the treatment of either of them alone. *Tdo2* and *Cyp2d10* were slightly induced by the combination of DAPT with C/EBPα. Although the level of expression of hepatocyte markers was much lower than in MHs, C/EBPα expression affected the differentiation status of mature cholangiocytes.

Grainyhead-like 2 inhibits hepatocytic differentiation

Overexpression of C/EBPα only slightly promoted hepatocytic differentiation. Therefore, we assumed that molecular machinery strongly stabilizing the cholangiocyte lineage might exist in adult cholangiocytes. As candidates of inhibitory factors, we examined expression of cholangiocytic transcription factors including Sox9, hairy enhance of slit 1 (Hes1), Hey1 and grainyhead like 2 (Grhl2) that we identified as cholangiocyte specific transcription factors (Senga et al., 2012). Their expression was higher in adult cholangiocytes than in neonatal cells (Fig. 4A). Furthermore, Grhl2 and Hes1 were maintained at lower levels in neonatal cells than in adult cells during culture (Fig. 4B). Interestingly, Grhl2 expression was further inhibited in neonatal culture after inducing hepatocytic differentiation by sequential treatment with OSM and MG. Downregulation of Grhl2 in neonatal cholangiocytes and its continuous expression in adult cells during the culture were further confirmed by immunofluorescence analysis (supplementary material Fig. S7). Therefore, we considered the possibility that constant expression of Grhl2 in adult cholangiocytes might inhibit hepatocytic differentiation.

To test this hypothesis, we introduced Grhl2 into neonatal cholangiocytes and induced hepatocytic differentiation, and found that Grhl2 inhibited induction of hepatocyte markers (Fig. 4C). We further confirmed that Grhl2 blocked expression of albumin, CPSI, HNF4α, and C/EBPα proteins induced by OSM and MG (Fig. 4D). Moreover, the downregulation of Grhl2 by short interfering RNAs (siRNAs) in adult cholangiocytes slightly induced hepatocytic characteristics (supplementary material Fig. S8). These results suggest that maintenance of Grhl2 at a high level is a crucial factor fixing adult EpCAM$^+$ cells in the cholangiocyte lineage.

Epithelial characteristics of neonatal and adult cholangiocytes

Given that Grhl2 is implicated in maturation of cholangiocytes (Senga et al., 2012), we considered the possibility that neonatal and adult cholangiocytes might be different in terms of their maturation status as epithelial cells, although bile duct structures are formed in neonatal liver (Fig. 5A). To examine epithelial characteristics of cholangiocytes, we cultured them to develop monolayers, and first measured transepithelial resistance (TER). In the culture condition used here, cholangiocytes formed a monolayer during 2 days of incubation. During and after the formation of the monolayers by neonatal and adult cholangiocytes, values of TER increased and reached a plateau (supplementary material Fig. S9). After 4 days of incubation, the monolayer of adult cholangiocytes showed the higher TER value than that of neonatal cells (Fig. 5B). We also examined the efflux of 4 kDa fluoresceinisothiocyanato dextran (FITC dextran) and found that FITC dextran passed through the monolayer derived from neonatal cholangiocytes more readily than through that of adult cells (Fig. 5C). These results indicated that neonatal

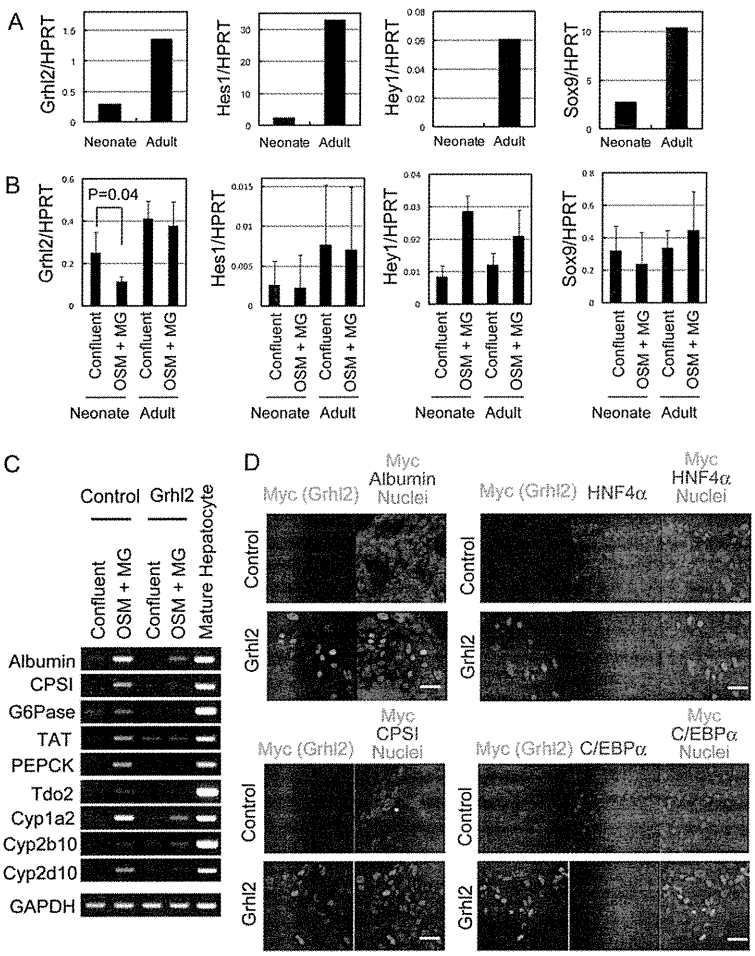

Fig. 4. Overexpression of Grhl2 inhibits hepatocyte conversion of neonatal cholangiocytes. (A) Cholangiocyte transcription factors are expressed more in neonatal cholangiocytes than in adult ones. Neonatal and adult cholangiocytes were isolated from 1W and 8W livers, respectively, as EpCAM$^+$ cells by FACS. Expressions of Grhl2, Hes1, Hey1 and Sox9 were examined by quantitative PCR. Neonatal and adult cholangiocytes were isolated from six and three mice, respectively, as EpCAM$^+$ cells by FACS. Cell isolation was repeated four times, independently. The expression levels are shown relative to that of adult cholangiocytes. (B) The expression of cholangiocyte transcription factors is changed during the culture of cholangiocytes. Expression of Grhl2 was downregulated in neonatal cholangiocytes during hepatocytic differentiation, whereas it was maintained in adult cells during culture. Expression of Hes1 in neonatal cholangiocytes remained at a lower level compared with adult cells. However, in contrast to Grhl2, Hes1 was not further downregulated during hepatocytic differentiation of neonatal cholangiocytes. Culture was repeated three times, independently. Error bars represent s.d. Two-tailed Student's *t*-tests were performed using Microsoft Excel. (C) Grhl2 inhibits hepatocytic differentiation of neonatal cholangiocytes. Grhl2 was introduced to neonatal cholangiocytes. Hepatocytic differentiation was induced by OSM and MG. Grhl2 inhibited the induction of hepatocytes markers. Cultures were repeated three times, independently. (D) Grhl2 inhibits expression of albumin, CPSI, HNF4α and C/EBPα proteins. Neonatal cholangiocytes introduced with the control vector or the vector containing Grhl2 were treated with OSM and MG. Expression of albumin, CPSI, HNF4α and C/EBPα was examined by immunostaining (red). Myc-tagged Grhl2 was detected by anti-Myc antibody (green). Scale bars: 50 μm.

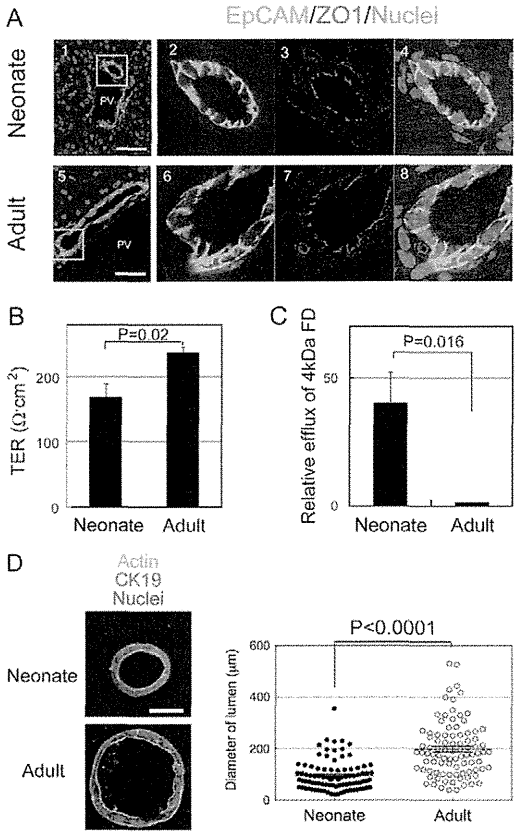

Fig. 5. Neonatal cholangiocytes are immature epithelial cells as compared with adult cells. (A) Bile ducts are present in neonatal and adult livers. EpCAM^{+} cholangiocytes form bile ducts in neonatal (1W-old) and adult livers. Tight junctions, recognized by ZO1 staining, are present around the lumens of neonatal and adult bile ducts. Liver sections were incubated with anti-EpCAM (green) and anti-ZO1 (red) antibodies. Nuclei were counterstained by Hoechst 33258. Boxes in panels 1 and 5 are enlarged in panels 2 4 and 6 8, respectively. Scale bars: 50 μm. (B) Neonatal cholangiocytes have a lower TER value. Fifty thousand cholangiocytes were plated onto Col-I gel in a 12-well plate. TER values at day 4 are shown in the graph. Cultures were repeated three times, independently. Bars indicate s.e.m. Two-tailed Student's *t*-tests were performed. (C) Higher paracellular efflux of 4 kDa FD occurs through the monolayer of neonatal cholangiocytes. At day 4 of culture, paracellular efflux of 4 kDa FITC-dextran (FD) was examined for the monolayers of neonatal and adult cholangiocytes. Bars indicate s.e.m. Two-tailed Student's *t*-tests were performed. (D) Neonatal cholangiocytes form smaller cysts than adult cells in 3D culture. Neonatal and adult cholangiocytes dissociated from Col-I gel were incubated in gel containing 5% Matrigel. Representative neonatal and adult cysts are shown in the left panels. Scale bar: 50 μm. After incubation for 10 days, the diameter of the lumen was measured. Cultures of neonatal and adult cholangiocytes were repeated three and two times, respectively. Each culture was performed in four wells. A dot plot is shown with bars indicating the means ± s.e.m.

cholangiocytes formed relatively immature tight junctions (TJs) compared with adult cells.

As we previously reported, maturation of TJs promotes epithelial morphogenesis, which could be correlated with enlargement of the apical lumen of cysts formed in three dimensional culture of epithelial cells (Senga et al., 2012). After 10 days of three dimensional culture, about 1% of neonatal and adult cholangiocytes formed cysts with a central lumen. However, the lumen size of neonatal cysts was significantly ($P<0.0001$) smaller than that of adult cysts, further suggesting that neonatal cells form relatively immature TJs compared with adult ones (Fig. 5D). These results indicate that neonatal cholangiocytes are immature epithelial cells.

Discussion

In this study, we demonstrated that cholangiocytes possess the ability to convert into hepatocytes in the neonatal period but this capability is lost in the adult. Similarly, it has been demonstrated that pancreatic duct cells have the potential to differentiate into endocrine and exocrine cells in the neonatal period but their differentiation potential becomes limited in the adult (Kopp et al., 2011). Thus, tubular epithelial cells may generally lose lineage plasticity during postnatal development.

Although, as we mentioned above, it has been shown that neonatal pancreatic duct cells lose the capability to differentiate to multiple types of cell during development, it is not known how the plasticity of epithelial cells is limited. We unexpectedly found that neonatal cholangiocytes are still developing epithelial characteristics even after forming the tubular structure. It can be assumed that production of bile by neonatal hepatocytes is less than that by mature ones and, therefore, relatively immature TJs in neonatal livers are sufficient to prevent the leakage of bile to the parenchyma and/or to the blood vessels, including the portal vein and the hepatic artery. This assumption seems to be consistent with the fact that the accumulation of bile in the neonatal gallbladder is much less than in the adult one (supplementary material Fig. S10). Furthermore, we showed that Grhl2 was expressed at a higher level in adult than in neonatal cholangiocytes and could inhibit hepatocytic differentiation. As we previously demonstrated, Grhl2 promotes formation of functional TJs by establishing a molecular network among claudin 3, claudin 4 and Rab25 (Senga et al., 2012). Thus, our results suggest that the molecular machinery that establishes the epithelial integrity limits the differentiation potential of epithelial cells and thereby stabilizes the lineage of the cells.

It was recently shown that transcription factors could covert fibroblasts into pluripotent stem cells or other types of somatic cells (Yamanaka and Blau, 2010; Yang, 2011). The combination of Gata4, HNF1α and FoxA1, or that of HNF4α plus FoxA1, A2 or A3, was able to convert mouse skin fibroblasts to hepatocytes (Huang et al., 2011; Sekiya and Suzuki, 2011). Because these proteins are strongly expressed in MHs but not in cholangiocytes, we considered the possibility that their expression status is a key to determining the potential for hepatocytic differentiation. In addition to these transcription factors, we focused on C/EBPα, which is also important for the functions of MHs (Inoue et al., 2004). During the course of hepatocytic differentiation, neonatal cholangiocytes expressed FoxA1, HNF4α and C/EBPα. Adult cholangiocytes, however, expressed FoxA1 but neither HNF4α nor C/EBPα. To elucidate the difference in induction, we examined epigenetic modification of the promoters of HNF4α and C/EBPα. Compared with hepatocytes, methylation of CpG sequences increased in cholangiocytes (supplementary material Fig. S11). However, there was little difference between 1W and 6W cholangiocytes. Other epigenetic mechanisms or upstream factors may regulate the expression of HNF4α and C/EBPα in hepatic epithelial cells. Although C/EBPα expression was effective in conferring hepatocytic characters on cholangiocytes,

the level of induction was limited. This indicates that other factors may block lineage conversion. The present study suggests that Grhl2 is one such inhibitory factor.

Although Grhl2 did not affect expression of C/EBPα mRNA, it did block induction of C/EBPα protein during hepatocytic differentiation (supplementary material Fig. S12; Fig. 4), suggesting that Grhl2 or its target inhibits translation of C/EBPα. However, downregulation of Grhl2 alone did not markedly induce expression of C/EBPα and hepatocytic differentiation in adult cholangiocytes. This result indicates that other molecules might be involved in regulating those processes. Nevertheless, when upregulation of C/EBPα and downregulation of Grhl2 simultaneously occurred in adult cholangiocytes, hepatocytic markers were further upregulated and some cells expressed albumin and CPSI proteins (supplementary material Fig. S13). Moreover, we demonstrated that the inhibition of the Notch pathway by DAPT was effective in inducing hepatocytic characteristics in adult cholangiocytes, although DAPT treatment only slightly upregulated Hes1. Given that the Notch pathway could regulate the lineage of hepatic epithelial cells independently of Hes1 (Jeliazkova et al., 2013), other targets of the pathway may be also involved in conferring hepatocytic characteristics in adult cholangiocytes. Taken together our results suggest that to induce hepatocytic differentiation in adult cholangiocytes, we may need to not only promote expression of hepatocytic transcription factors but also inhibit cholangiocytic factors and the Notch pathway.

In summary, we demonstrate here that cholangiocytes alter their lineage plasticity during epithelial maturation. We identified a possible molecular network augmenting epithelial structures and functions, which also contributes to stabilization of the epithelial cell lineage by blocking conversion to other lineages. Our results suggest that it is not easy to convert the mass of mature cholangiocytes to hepatocytes; however, several groups have reported that hepatocytes can be produced from pluripotent stem cells or somatic cells (Si Tayeb et al., 2010; Huang et al., 2011; Sekiya and Suzuki, 2011). Although induced hepatocytes differentiate to functional hepatocytes in diseased mice, it is still difficult to control the process of hepatocytic differentiation of pluripotent and somatic cells and produce a mass of MHs *in vitro*. Neonatal cholangiocytes have a remarkably strong ability to convert into hepatocytes, so for pluripotent cells to achieve the differentiation status of these cells would be an important step in the differentiation process. We have successfully expanded human cholangiocytes isolated from adult human liver tissue in the same culture conditions as used for mouse cholangiocytes (supplementary material Fig. S3). In addition, cholangiocytes isolated from extrahepatic bile ducts and the gallbladder of adult mice could proliferate efficiently in the same culture conditions (data not shown). Therefore, if we could find a factor that reverts mature cholangiocytes to the differentiation status of neonatal ones, it may be possible to produce functional hepatocytes that can be used as a source of cell therapy and for drug screening.

Materials and Methods

Extracellular matrix, growth factors and chemicals

Col-I (3 mg/ml) was purchased from Koken Co., Ltd (Tokyo, Japan). Growth factor-reduced Matrigel® (MG), which contains extracellular matrix proteins including type IV collagen, laminin-111 and nidogen, was purchased from BD Biosciences (Bedford, MA). Epidermal growth factor (EGF), hepatocyte growth factor (HGF) and OSM were purchased from R&D Systems (Minneapolis, MN).

Isolation and culture of cholangiocytes

One-week (1W)- and 6-week (6W)- old mice (C57BL6, Sankyo Lab Service, Japan) were used to isolate neonatal and adult cholangiocytes, respectively. All the animal experiments were approved by the Sapporo Medical University Institutional Animal Care and Use Committee and were carried out under the institutional guidelines for ethical animal use. A two-step collagenase perfusion method was performed through the portal vein of adult mice or through the left ventricle of neonatal mice to digest liver tissues. After the removal of parenchymal cells, the residual material including bile ducts was further digested with Liberase TM (Roche Applied Sciences, San Diego, CA) for neonatal tissues or with collagenase/hyaluronidase solution for adult tissues. Enzymatic digestion was terminated by adding ice-cold fresh medium containing 10% fetal bovine serum (FBS).

The cell suspension was passed sequentially through a 100-μm mesh and a 70-μm cell strainer (BD Biosciences). Nonspecific binding of antibodies was blocked by an antibody against the Fcγ receptor (anti-CD16/CD32 antibody; BD Biosciences). Cells were incubated with biotin-conjugated anti-EpCAM antibody (BioLegend, San Diego, CA) followed by streptavidin microbeads (Miltenyi Biotec, Gladbach, Germany). $EpCAM^+$ cells were purified through a MACS column (Miltenyi Biotec). Twenty thousand cells were placed in each well of a 12-well plate. For culture on Col-I gel or MG, collagen type IAC (Koken) mixed with 10× reconstitution buffer containing 200 mM HEPES, 50 mM NaOH, 260 mM $NaHCO_3$, 10× Dulbecco's modified Eagle's medium (DMEM) and PBS or MG was added to each well. To coat wells with collagen type IAC or MG, these agents were diluted in 0.1 M CH_3COOH and DMEM/F12 medium, respectively, and 500 μl of solution was added to each well. The cells were cultured in DMEM/F12 medium supplemented with 10% FBS, 10 ng/ml EGF and HGF, 5×10^{-8} M dexamethasone (Dex; Sigma Chemical Co., St. Louis, MO) and 1× insulin-transferrin-selenium (ITS; Gibco, Carlsbad, CA). After 5–7 days in culture, cells were dissociated from the dishes and then used for subculture (supplementary material Fig. S1).

Human liver tissue was obtained from a patient who underwent hepatic resection at Sapporo Medical University Hospital, with informed consent and the approval of the Sapporo Medical University Ethics Committees. The liver tissue was digested by a method reported previously (Sasaki et al., 2008). Cholangiocytes were isolated from the remaining tissue using the same protocol as that used for the isolation of mouse cholangiocytes and then purified through an MACS column with FITC-conjugated anti-human EpCAM (BioLegend) and anti-FITC microbeads (Miltenyi Biotec).

Induction of hepatocytic differentiation

After culture on Col-I gel, cholangiocytes were dissociated from the gel and 5×10^4 cells were cultured in each well of 24-well plates coated with gelatin. After the cells became confluent, they were incubated with 20 ng/ml OSM, 1% DMSO, 10^{-7} M Dex, and 1× ITS for 4 days and then overlaid with 5% MG for an additional 4 days.

To examine the ability to eliminate ammonium ions from the culture medium, NH_4Cl was added to the culture medium at 2 mM. The concentration of ammonium ions was measured every 2 hours by using the Ammonia Test Wako (Wako Pure Chemical Industries, Osaka, Japan).

To enhance the formation of bile canaliculus (BC) structures in the colonies, 100 μM taurocholate (Tokyo Chemical Industry Co. Ltd, Tokyo, Japan) was added to the medium for 1 day. The formation of BC-like structures was confirmed by incubation with 10 μg/ml fluorescein diacetate (FDA; Sigma-Aldrich, St. Louis, MO) for 30 minutes. The accumulation of metabolized fluorescein into BC-like structures was examined.

Overexpression of transcription factors

cDNAs of C/EBPα, HNF 4α and Grhl2 were amplified by PCR and inserted into retroviral vectors to generate pMXsNeo-C/EBPα, pMXsPuro-HNF4α and pMXsNeo-Grhl2. Retrovirus was added to the culture 48 hours after starting the culture on Col-I gel. For the control, pMXsNeo or pMXsPuro was introduced to cholangiocytes. G418 (1 mg/ml) or puromycin (10 μg/ml) was added to the culture 24 hours after infection to select cells with pMXsNeo-C/EBPα or pMXsNeo-Grhl2, and pMXsPuro-HNF4α, respectively. After incubation in the presence of antibiotics for 24 hours, cells were incubated in medium without them for 2 or 3 days before replating onto gelatin-coated dishes.

PCR

Total RNA was isolated from purified $EpCAM^+$ cells using an RNeasy Mini Kit (Qiagen, Hilden, Germany). cDNA was synthesized using an Omniscript Reverse Transcription Kit (Qiagen). Primers used for PCR are shown in supplementary material Table S1.

Immunofluorescence chemistry

Cholangiocytes induced to differentiate or colonies derived from $EpCAM^+$ cells were fixed in PBS containing 4% paraformaldehyde (PFA) at 4°C for 15 minutes.

After permeabilization with 0.2% Triton X-100 and blocking with Blockace (DS Pharma, Biomedical Co. Ltd, Osaka, Japan), cells were incubated with primary antibodies (supplementary material Table S2). Signals were visualized with Alexa-Fluor-488, -555 or -633-conjugated secondary antibodies (Molecular Probes, Carlsbad, CA). Nuclei were counterstained with Hoechst 33258. Images were acquired with a Nikon X-81 fluorescence microscope.

Measurement of TER and paracellular tracer flux

Fifty thousand cholangiocytes dissociated from the Col-I gel were replated on a 12 mm Transwell with a 0.4 μm pore, polyester membrane coated with Col-I gel, which was placed in a 12-well plate (Corning Inc., Corning, NY). TER was measured directly in the culture medium using a Millicell-ERS epithelial Volt Ohm meter (Millipore, Billerica, MA) during the culture. The TER values were calculated by subtracting the background TER of blank filters, followed by multiplying by the surface area of the filter (1.12 cm^2). For the paracellular tracer flux assay, 4 kDa FITC-dextran (Sigma-Aldrich) was added to the medium inside the Transwell dish on day 4 at a concentration of 1 mg/ml. After incubation for 2 hours, an aliquot of medium was collected from the basal compartment. The paracellular tracer flux was determined as the amount of FITC-dextran in the basal medium, which was measured with an Infinite M1000 Pro multi-plate reader (Tecan Group Ltd, Mannedorf, Switzerland).

Three-dimensional culture

Neonatal and adult cholangiocytes were cultured in gel containing Matrigel® as previously reported (Tanimizu et al., 2007). Briefly, cholangiocytes were dissociated from Col-I gel and 5,000 cells were replated on the mixture of Matrigel® and type I collagen (1:1 v/v) in a well of an 8-well coverglass chamber (Nunc, Roskilde, Denmark) covered with 5% Matrigel®. After 5 minutes of incubation, cells were fixed and used for immunofluorescence analysis.

Acknowledgements

We thank Ms Minako Kuwano and Ms Yumiko Tsukamoto for technical assistance.

Author contributions

N.T., study concept and design, acquisition and analysis of data, writing the manuscript, obtained funding; Y.N., sample preparation; N.I., discussion about data, T.M., sample preparation and obtained funding; K.H., obtained funding; T.M., editing the manucscript, obtained funding.

Funding

This work was supported by the Ministry of Education, Culture, Sports, Science and Technology, Japan, Grants in Aid for Young Scientists (B) [grant number 22790386 to N.T.]; Innovative Area [grant number 24112519 to N.T.]; and Grants in Aid for Scientific Research (B) [grant numbers 22390259 to K.H. and 21390365, 24390304 to T.M.].

Supplementary material available online at
http://jcs.biologists.org/lookup/suppl/doi:10.1242/jcs.133082/-/DC1

References

Espanol-Suner, R., Carpentier, R., Van Hul, N., Legry, V., Achouri, Y., Cordi, S., Jacquemin, P., Lemaigre, F. and Leclercq, I. A. (2012). Liver progenitor cells yield functional hepatocytes in response to chronic liver injury in mice. *Gastroenterology* **143**, 1564-1575, e1567.

Fu, D., Wakabayashi, Y., Lippincott-Schwartz, J. and Arias, I. M. (2011). Bile acid stimulates hepatocyte polarization through a cAMP-Epac-MEK-LKB1-AMPK pathway. *Proc. Natl. Acad. Sci. USA* **108**, 1403-1408.

Huang, P., He, Z., Ji, S., Sun, H., Xiang, D., Liu, C., Hu, Y., Wang, X. and Hui, L. (2011). Induction of functional hepatocyte-like cells from mouse fibroblasts by defined factors. *Nature* **475**, 386-389.

Inoue, Y., Inoue, J., Lambert, G., Yim, S. H. and Gonzalez, F. J. (2004). Disruption of hepatic C/EBPalpha results in impaired glucose tolerance and age-dependent hepatosteatosis. *J. Biol. Chem.* **279**, 44740-44748.

Jeliazkova, P., Jors, S., Lee, M., Zimber-Strobl, U., Ferrer, J., Schmid, R. M., Siveke, J. T. and Geisler, F. (2013). Canonical Notch2 signaling determines biliary cell fates of embryonic hepatoblasts and adult hepatocytes independent of Hes1. *Hepatology* **57**, 2469-2479.

Kopp, J. L., Dubois, C. L., Hao, E., Thorel, F., Herrera, P. L. and Sander, M. (2011). Progenitor cell domains in the developing and adult pancreas. *Cell Cycle* **10**, 1921-1927.

Mackey, S. L. and Darlington, G. J. (2004). CCAAT enhancer-binding protein alpha is required for interleukin-6 receptor alpha signaling in newborn hepatocytes. *J. Biol. Chem.* **279**, 16206-16213.

Malato, Y., Naqvi, S., Schürmann, N., Ng, R., Wang, B., Zape, J., Kay, M. A., Grimm, D. and Willenbring, H. (2011). Fate tracing of mature hepatocytes in mouse liver homeostasis and regeneration. *J. Clin. Invest.* **121**, 4850-4860.

Michalopoulos, G. K. (2007). Liver regeneration. *J. Cell. Physiol.* **213**, 286-300.

Michalopoulos, G. K. (2011). Liver regeneration: alternative epithelial pathways. *Int. J. Biochem. Cell Biol.* **43**, 173-179.

Nishikawa, Y., Doi, Y., Watanabe, H., Tokairin, T., Omori, Y., Su, M., Yoshioka, T. and Enomoto, K. (2005). Transdifferentiation of mature rat hepatocytes into bile duct-like cells in vitro. *Am. J. Pathol.* **166**, 1077-1088.

Oertel, M., Rosencrantz, R., Chen, Y. Q., Thota, P. N., Sandhu, J. S., Dabeva, M. D., Pacchia, A. L., Adelson, M. E., Dougherty, J. P. and Shafritz, D. A. (2003). Repopulation of rat liver by fetal hepatoblasts and adult hepatocytes transduced ex vivo with lentiviral vectors. *Hepatology* **37**, 994-1005.

Parviz, F., Matullo, C., Garrison, W. D., Savatski, L., Adamson, J. W., Ning, G., Kaestner, K. H., Rossi, J. M., Zaret, K. S. and Duncan, S. A. (2003). Hepatocyte nuclear factor 4alpha controls the development of a hepatic epithelium and liver morphogenesis. *Nat. Genet.* **34**, 292-296.

Sasaki, K., Kon, J., Mizuguchi, T., Chen, Q., Ooe, H., Oshima, H., Hirata, K. and Mitaka, T. (2008). Proliferation of hepatocyte progenitor cells isolated from adult human livers in serum-free medium. *Cell Transplant.* **17**, 1221-1230.

Sastre, M., Steiner, H., Fuchs, K., Capell, A., Multhaup, G., Condron, M. M., Teplow, D. B. and Haass, C. (2001). Presenilin-dependent gamma-secretase processing of beta-amyloid precursor protein at a site corresponding to the S3 cleavage of Notch. *EMBO Rep.* **2**, 835-841.

Sekine, K., Chen, Y. R., Kojima, N., Ogata, K., Fukamizu, A. and Miyajima, A. (2007). Foxo1 links insulin signaling to C/EBPalpha and regulates gluconeogenesis during liver development. *EMBO J.* **26**, 3067-3615.

Sekiya, S. and Suzuki, A. (2011). Direct conversion of mouse fibroblasts to hepatocyte-like cells by defined factors. *Nature* **475**, 390-393.

Sekiya, T., Muthurajan, U. M., Luger, K., Tulin, A. V. and Zaret, K. S. (2009). Nucleosome-binding affinity as a primary determinant of the nuclear mobility of the pioneer transcription factor FoxA. *Genes Dev.* **23**, 804-809.

Senga, K., Mostov, K. E., Mitaka, T., Miyajima, A. and Tanimizu, N. (2012). Grainyhead-like 2 regulates epithelial morphogenesis by establishing functional tight junctions through the organization of a molecular network among claudin3, claudin4, and Rab25. *Mol. Biol. Cell* **23**, 2845-2855.

Si-Tayeb, K., Noto, F. K., Nagaoka, M., Li, J., Battle, M. A., Duris, C., North, P. E., Dalton, S. and Duncan, S. A. (2010). Highly efficient generation of human hepatocyte-like cells from induced pluripotent stem cells. *Hepatology* **51**, 297-305.

Tanimizu, N. and Miyajima, A. (2004). Notch signaling controls hepatoblast differentiation by altering the expression of liver-enriched transcription factors. *J. Cell Sci.* **117**, 3165-3174.

Tanimizu, N., Nishikawa, M., Saito, H., Tsujimura, T. and Miyajima, A. (2003). Isolation of hepatoblasts based on the expression of Dlk/Pref-1. *J. Cell Sci.* **116**, 1775-1786.

Tanimizu, N., Miyajima, A. and Mostov, K. E. (2007). Liver progenitor cells develop cholangiocyte-type epithelial polarity in three-dimensional culture. *Mol. Biol. Cell* **18**, 1472-1479.

Yamanaka, S. and Blau, H. M. (2010). Nuclear reprogramming to a pluripotent state by three approaches. *Nature* **465**, 704-712.

Yamasaki, H., Sada, A., Iwata, T., Niwa, T., Tomizawa, M., Xanthopoulos, K. G., Koike, T. and Shiojiri, N. (2006). Suppression of C/EBPalpha expression in periportal hepatoblasts may stimulate biliary cell differentiation through increased Hnf6 and Hnf1b expression. *Development* **133**, 4233-4243.

Yang, L. (2011). From fibroblast cells to cardiomyocytes: direct lineage reprogramming. *Stem Cell Res. Ther.* **2**, 1.

Zong, Y., Panikkar, A., Xu, J., Antoniou, A., Raynaud, P., Lemaigre, F. and Stanger, B. Z. (2009). Notch signaling controls liver development by regulating biliary differentiation. *Development* **136**, 1727-1739.

HEPATOLOGY
Official Journal of the American Association for the Study of Liver Diseases
AASLD

Differentiation Capacity of Hepatic Stem/Progenitor Cells Isolated From D-Galactosamine-Treated Rat Livers

Norihisa Ichinohe,[1] Naoki Tanimizu,[1] Hidekazu Ooe,[1] Yukio Nakamura,[1,2] Toru Mizuguchi,[2] Junko Kon,[1] Koichi Hirata,[2] and Toshihiro Mitaka[1]

Oval cells and small hepatocytes (SHs) are known to be hepatic stem and progenitor cells. Although oval cells are believed to differentiate into mature hepatocytes (MHs) through SHs, the details of their differentiation process are not well understood. Furthermore, it is not certain whether the induced cells possess fully mature functions as MHs. In the present experiment, we used Thy1 and CD44 to isolate oval and progenitor cells, respectively, from D-galactosamine-treated rat livers. Epidermal growth factor, basic fibroblast growth factor, or hepatocyte growth factor could trigger the hepatocytic differentiation of sorted Thy1$^+$ cells to form epithelial cell colonies, and the combination of the factors stimulated the emergence and expansion of the colonies. Cells in the Thy1$^+$-derived colonies grew more slowly than those in the CD44$^+$-derived ones *in vitro* and *in vivo* and the degree of their hepatocytic differentiation increased with CD44 expression. Although the induced hepatocytes derived from Thy1$^+$ and CD44$^+$ cells showed similar morphology to MHs and formed organoids from the colonies similar to those from SHs, many hepatic differentiated functions of the induced hepatocytes were less well performed than those of mature SHs derived from the healthy liver. The gene expression of cytochrome P450 1A2, tryptophan 2,3-dioxygenase, and carbamoylphosphate synthetase I was lower in the induced hepatocytes than in mature SHs. In addition, the protein expression of CCAAT/enhancer-binding protein alpha and bile canalicular formation could not reach the levels of production of mature SHs. *Conclusion*: The results suggest that, although Thy1$^+$ and CD44$^+$ cells are able to differentiate into hepatocytes, the degree of maturation of the induced hepatocytes may not be equal to that of healthy resident hepatocytes. (HEPATOLOGY 2012; 57:1192-1202)

The liver normally exhibits a very low level of cell turnover, but when loss of mature hepatocytes (MHs) occurs, a rapid regenerative response is elicited from all cell types in the liver to restore the organ to its initial state. The loss may occur as a result of toxic injury, viral infection, trauma, or surgical resection. Because hepatocytes are the major functional cells of the liver, large-scale hepatocytic loss becomes a trigger for regeneration, and replication of existing hepatocytes is generally the quickest, most efficient way to compensate for the lost functions. However, when the replication of hepatocytes is delayed or entirely inhibited, hepatic stem/progenitor cells (HPCs) are activated.[1-3] As HPCs, oval cells and small hepatocytes (SHs) are well known. Oval cells were first reported to be cells that possessed an ovoid nucleus and

Abbreviations: Abs, antibodies; AFP, alpha-fetoprotein; Alb, albumin; BC, bile canaliculus; bFGF, basic fibroblast growth factor; BrdU, 5-bromo-2'-deoxyuridine; BW, body weight; CPS-I, carbamoylphosphate synthetase I; CK, cytokeratin; C/EBP, CCAAT/enhancer-binding protein; CYP1A2, cytochrome P450 1A2; 3D, three-dimensional; DPPIV, dipeptidylpeptidase IV; ECM, extracellular matrix; EGF, epidermal growth factor; FD, fluorescent diacetate; FGF, fibroblast growth factor; GalN, D-galactosamine; HA, hyaluronic acid; HGF, hepatocyte growth factor; HNF, hepatocyte nuclear factor; HPCs, hepatic stem/progenitor cells; ICC, immunocytochemistry; INF-γ, interferon-gamma; IP, intraperitoneally; LI, labeling index; MH, mature hepatocyte; mRNA, messenger RNA; PBS, phosphate-buffered saline; PH, partial hepatectomy; qPCR, quantitative polymerase chain reaction; RET, retrorsine; SH, small hepatocyte; TAT, tyrosine aminotransferase; TGF, transforming growth factor; TNF-α, tumor necrosis factor alpha; TDO, tryptophan 2,3-dioxygenase;

From the [1]Department of Tissue Development and Regeneration, the Research Institute for Frontier Medicine, and [2]First Department of Surgery, Sapporo Medical University School of Medicine, Sapporo, Japan.

Received January 31, 2012; accepted September 8, 2012.

This work was supported by the Ministry of Education, Culture, Sports, Science, and Technology, Japan, Grant-in-Aid for Scientific Research (C) (19566021; to N.I.), Grants-in-Aid for Young Scientists (B) (22790385, to N.I.; and 19790294, to J.K.), a grant from the Yuasa Memorial Foundation (to T.M.), and Grants-in-Aid for Scientific Research (B) (22390259, to K.H.; and 21390365, to T.M.), a program for developing the supporting system for upgrading the education and research (to T.M.).

Dr. Kon is currently affiliated with Gene Techno Science Co. Ltd., Sapporo, Japan.

scant cytoplasm.[4] The appearance of oval cells has been reported in rat livers treated with hepatotoxins, such as 2-acetylaminofluorene (2-AAF), combined with partial hepatectomy (PH) and D-galactosamine (GalN).[1,5–7] In GalN-induced rat liver injury, it has been shown that oval cells appear in the periportal area and differentiate into MHs through basophilic small-sized ones.[8,9] Oval cells show a wide range of phenotypic heterogeneity, and cytokeratins (CKs) 7 and 19, alpha-fetoprotein (AFP), CD34, c-kit, and Thy1 have been reported as markers for them.[1,2,5–7]

On the other hand, SHs are a subpopulation of hepatocytes, and cells isolated from healthy adult rats[10,11] and human livers[12] can clonally proliferate to form colonies and differentiate into MHs *in vitro*.[11,13] Recently, we identified CD44 as a specific marker of SHs.[14] In GalN-treated rat livers, $CD44^+$ cells appear near the periportal area between $Thy1^+$ oval cells and resident hepatocytes soon after the emergence of $Thy1^+$ oval cells.[15] In addition, we previously showed that $Thy1^+$ oval cells differentiate into hepatocytes through $CD44^+$ cells.[15,16] Our data suggested that cells sequentially converted from $Thy1^+CD44^-$ to $Thy1^+CD44^+$ and then to $Thy1^-CD44^+$ cells during the process of hepatocytic differentiation of oval cells.[15,16] Furthermore, sorted $Thy1^+$ and $CD44^+$ cells could repopulate host livers when they were transplanted into rat livers treated with retrorsine (RET) and two-thirds PH.

Although most oval cells are thought to differentiate into MHs, the details of their differentiation process, such as factors for hepatic commitment, characteristics of intermediate cells, and their fates are not well understood. In addition, it has not been elucidated whether the induced hepatocytes differentiate to possess the same capabilities as MHs. In the present experiment, we aimed to clarify which factors might induce hepatocytic differentiation of $Thy1^+$ cells and to examine how $Thy1^+$ cells could differentiate into hepatocytes through $CD44^+$ cells. In addition, we examined whether the $Thy1^+$ and $CD44^+$ cells could differentiate into fully MHs, as with those in the healthy adult liver.

Materials and Methods

Animals and Liver Injury Model. Male F344 rats (dipeptidylpeptidase IV [DPPIV]$^+$ strain; Sankyo Lab Service Corporation, Inc., Tokyo, Japan), weighing 150-200 g, were used. All animals received humane care, and the experimental protocol was approved by the committee on laboratory animals according to Sapporo Medical University guidelines. For GalN-injured livers, GalN (75 mg/100 g body weight [BW] dissolved in phosphate-buffered saline [PBS]; Acros, Geel, Belgium) was intraperitoneally (IP) administered.[14] For the transplantation experiment, female F344 rats (DPPIV strain; Charles River Laboratories, Wilmington, MA) were (IP) given two injections of RET (30 mg/kg BW; Sigma-Aldrich Chemical Co., St. Louis, MO), 2 weeks apart,[17] and 4 weeks after the second injection, two-thirds PH was performed (RET/PH liver). Sorted $DPPIV^+$ cells (5×10^5 cells/0.5 mL) were transplanted into RET/PH livers (DPPIV) through the spleen (at least 3 rats per group).

Isolation and Culture of Cells. Rats were used to isolate hepatic cells by the collagenase perfusion method, as previously described.[18] After perfusion, the cell suspension was centrifuged at $50 \times g$ for 1 minute. The supernatant and the precipitate were used for sorting $Thy1^+$ and $CD44^+$ cells and preparing MHs, respectively. The procedure used for cell sorting was as previously described,[15] with some modifications. Antibodies (Abs) used for cell sorting are listed in Supporting Table 1. $Thy1^+CD44^+$ cells were sorted from $CD44^+$ cell and $Thy1^+$ cell fractions by using anti-Thy1 or CD44 Abs, respectively, and both were pooled. Furthermore, $Thy1^+$ and $CD44^+$ cells were also separated from $CD44^-$ and $Thy1^-$ cell fractions, respectively. After the number of viable cells was counted, 1×10^5 viable cells were plated in 12-well plates (Corning Inc., Corning, NY) and cultured in the medium listed in Supporting Table 2. The medium was replaced with fresh medium thrice-weekly.

To examine whether cells in the colonies could fully differentiate into MHs and form functional bile canaliculi (BCs), $Thy1^+CD44^-$ and $Thy1^-CD44^+$ cells sorted from GalN-D3 and SHs derived from a healthy liver were cultured for 10 days. Thereafter, some dishes were treated with Matrigel (BD Biosciences, San Diego, CA) for 10 days. To enhance the organoid formation of the colonies, as previously reported,[19]

Address reprint requests to: Norihisa Ichinohe, D.D.S., Ph.D., Department of Tissue Development and Regeneration, Research Institute for Frontier Medicine, Sapporo Medical University School of Medicine, South-1, West-17, Chuo-ku, Sapporo 060-8556, Japan. E-mail: nichi@sapmed.ac.jp; fax: +81-11-615-3099.

View this article online at wileyonlinelibrary.com.
DOI 10.1002/hep.26084
Potential conflict of interest: Nothing to report.
Additional Supporting Information may be found in the online version of this article.